Bioconjugate Chemistry

Article

pubs.acs.org/bc

RGD Labeled Ru(II) Polypyridyl Conjugates for Platelet Integrin $\alpha_{IIb}\beta_3$ Recognition and as Reporters of Integrin Conformation

Kellie Adamson,[†] Ciaran Dolan,[†] Niamh Moran,[‡] Robert J. Forster,[†] and Tia E. Keyes*[,†]

[†]School of Chemical Sciences, Dublin City University, Dublin 9, Ireland

[‡]The Department of Molecular and Cellular Therapeutics, Royal College of Surgeons in Ireland, Dublin 2, Ireland

Supporting Information

ABSTRACT: The ability of two novel ruthenium(II) polypyridyl-Arg-Gly-Asp (RGD) peptide conjugates to act as molecular probes for reporting on the presence and conformation of integrin $\alpha_{IIb}\beta_3$ in solution and in live cells was described. The compounds are $[Ru(bpy)_2PIC\text{-}RGD]^{2+}$, bpy-RGD, and $[Ru(dpp)_2PIC\text{-}RGD]^{2+}$, dpp-RGD, where dpp is 4,7-diphenyl-1,10-phenanthroline, bpy is 2,2′-bipyridine, and PIC is 2-(4-carboxyphenyl)imidazo[4,5-*f*]-[1,10]phenanthroline. Bpy-RGD is hydrophilic, whereas dpp-RGD is comparatively hydrophobic. Both probes exhibited good affinity and high specificity for purified $\alpha_{IIb}\beta_3$ in solution. Binding of either complex to the resting integrin resulted in an approximately 8-fold increase of emission intensity from the metal center with dissociation constants (K_d) in the micromolar range for each complex. The K_d for each conjugate/$\alpha_{IIb}\beta_3$ assembly were compared following treatment of the integrin with the activating agents, Mn^{2+} and dithiothreitol (DTT), which are commonly used to induce active-like conformational changes in the integrin. For bpy-RGD/$\alpha_{IIb}\beta_3$ K_d showed relatively little variation with integrin activation, presenting the following trend: denatured $\alpha_{IIb}\beta_3$ > resting $\alpha_{IIb}\beta_3$ = pretreated DTT = pretreated Mn^{2+}. K_d for dpp-RGD/ $\alpha_{IIb}\beta_3$ showed greater variation with integrin activation and the following trend was followed: denatured $\alpha_{IIb}\beta_3$ > resting $\alpha_{IIb}\beta_3$ > pretreated Mn^{2+} = pretreated DTT. Time resolved luminescence anisotropy was carried out to obtain the rotational correlation time of bpy-RGD and dpp-RGD bound to resting or nominally activated integrin. The rotational correlation times of bpy-RGD and dpp-RGD, too fast to measure unbound, decreased to 1.50 ± 0.03 μs and 2.58 ± 0.04 μs, respectively, when the complexes were bound to resting integrin. Addition of Mn^{2+} to bpy-RGD/$\alpha_{IIb}\beta_3$ or dpp-RGD/$\alpha_{IIb}\beta_3$ reduced the rotational correlation time of the ruthenium center to 1.29 ± 0.03 μs and to 1.72 ± 0.03 μs, respectively. Following treatment, the rotational correlation time decreased to 1.04 ± 0.01 μs and 1.29 ± 0.03 μs for bpy-RGD/$\alpha_{IIb}\beta_3$, and dpp-RGD/$\alpha_{IIb}\beta_3$, respectively. The large relative changes in rotational correlation times observed for Mn^{2+} or DTT activated integrin indicates significant change in protein conformation compared with the resting integrin. The results also indicated that the metal complex itself affects the final conformational and/or aggregation status of the protein obtained. Furthermore, the extent of conformational change was influenced by whether the probe was bound to the integrin before or after activator treatment. Finally, in vitro studies indicated that both probes selectively bind to CHO cells expressing the resting form of $\alpha_{IIb}\beta_3$. In each case the probe colocalized with α_{IIb} specific SZ22 antibody. Overall, this work indicates that bpy-RGD and dpp-RGD may be useful peptide-probes for rapid assessment of integrin structural status and localization in solution and cells.

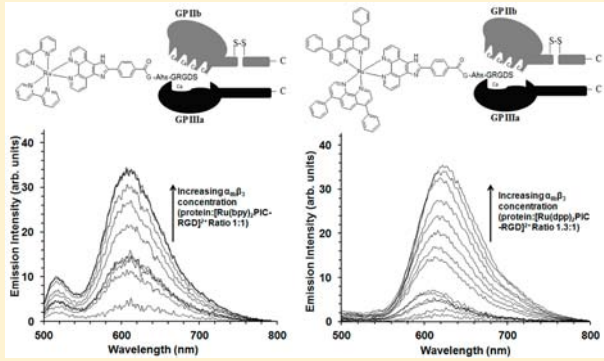

INTRODUCTION

The integrin $\alpha_{IIb}\beta_3$ (GPIIb/IIIa) is a heterodimeric glycoprotein cell adhesion receptor that lies across the plasma membrane of human platelets. Its physiological function is intimately linked to the process of platelet activation and thrombosis.[1] At least two conformational forms of $\alpha_{IIb}\beta_3$ are known to exist, each with different adhesion properties toward its primary ligand, fibrinogen. In its native or "resting" state $\alpha_{IIb}\beta_3$ is believed to assume a bent conformation with low binding affinity toward fibrinogen.[2] In its "activated" state, typically formed when platelets encounter physiologic stimuli such as ADP or thrombin via the inside-out mechanism, $\alpha_{IIb}\beta_3$ undergoes a gross conformational change and clustering at the platelet membrane. Its activated conformation exhibits high affinity for fibrinogen. The exact structural details of the conformational changes that can occur between the most extreme states of rest and activation in $\alpha_{IIb}\beta_3$ remain controversial, but the distinct difference between resting and fully activated conformations is well accepted.[2,3] For a full review of the integrin family, see references.[4−6] Fibrinogen (MW 340 kDa), the primary ligand for $\alpha_{IIb}\beta_3$,[7,8] contains three potential integrin binding sites: an RGD motif within the A_α

Received: February 20, 2014
Revised: April 8, 2014
Published: April 10, 2014

Scheme 1. Molecular Structures of (i) G-Ahx-GRGDS Peptide, the Parent Dyes (ii) $[Ru(bpy)_2PIC]^{2+}$, and (iii) $[Ru(dpp)_2PIC]^{2+}$ and Dye−Peptide Conjugates (iv) bpy-RGD and (v) dpp-RGD

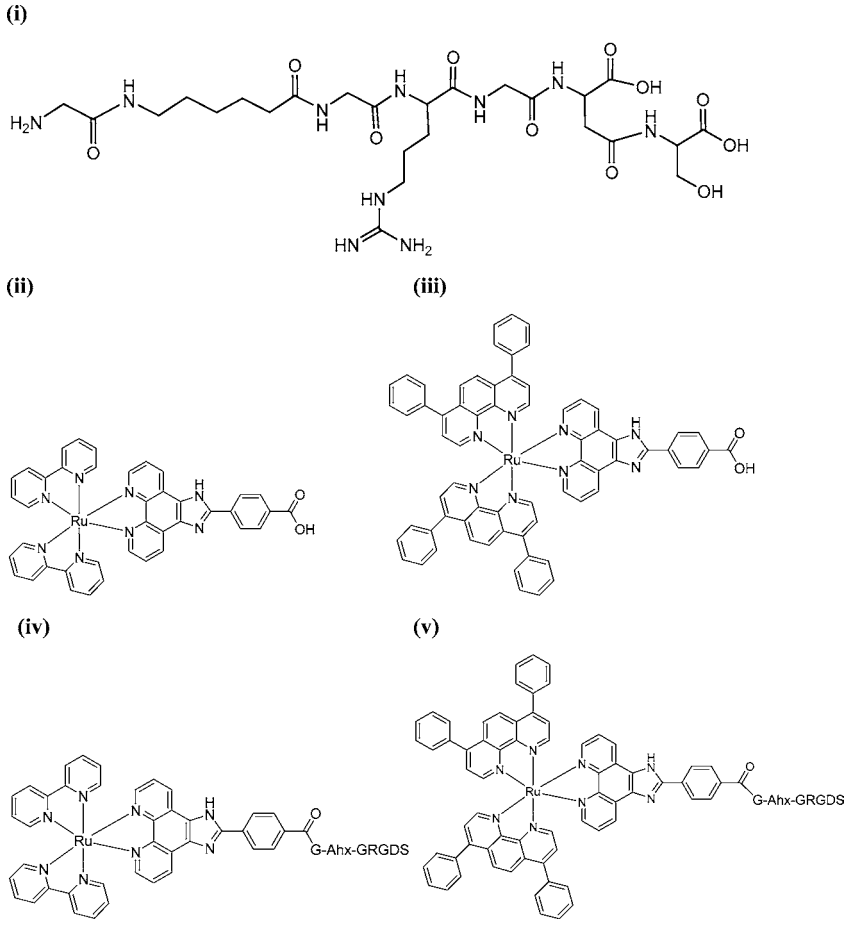

chain, $A_\alpha^{572-575}$ (RGDS), and a non-RGD dodecapeptide sequence in the γ chain (C-terminal $\gamma^{400-411}$). A second RGD motif exists, A_α $^{95-98}$ (RGDF) but it is thought that this motif is masked within a coil domain and so cannot participate in mediating platelet aggregation. Both RGDS and the non-RGD dodecapeptide $\gamma^{400-411}$ sequences mediate platelet aggregation by cross-linking $\alpha_{IIb}\beta_3$ receptors on adjacent platelets leading to thrombus formation. Because of its key role in thrombosis, $\alpha_{IIb}\beta_3$ is deemed the "central" integrin in thrombosis. However, beyond heart disease, platelet aggregation plays a key role in facilitating cancer metastases where platelets are known to cloak circulating tumor cells from immune response and $\alpha_{IIb}\beta_3$ plays an important role in this process.[9,10] Consequently, understanding $\alpha_{IIb}\beta_3$ behavior and identifying its "activation status" is crucial in predicting thrombotic risk and in advancing therapeutic approaches toward managing thrombosis and related diseases including cancer.

In addition to physiological stimuli, many chemical agents can induce $\alpha_{IIb}\beta_3$ activation.[11−14] These include the bifunctional reducing agent, DTT, divalent cations Mn^{2+}, EDTA (due to its chelation of the divalent cation Ca^{2+} from the integrin structure), and RGD-containing peptide drugs, e.g., Eptifibatide. Such chemical agents have provided key insights into the gross structural changes accompanying activation of $\alpha_{IIb}\beta_3$.[14,15] Although there is evidence that there is significant variation in conformational states induced depending on the chemical activators applied, there have been few systematic studies directed toward comparison of the conformational modifications following treatment of $\alpha_{IIb}\beta_3$ by the commonly employed chemical activators.[11]

This report addresses if Ru(II)polypyridyl complexes conjugated to a linear RGD peptide bind to and can, through modifications to their photophysical properties, reflect $\alpha_{IIb}\beta_3$ conformation and oligomerization in the resting and nominally activated $\alpha_{IIb}\beta_3$ states generated by Mn^{2+} or DTT treatment. The value of luminescence anisotropy to study integrin conformational change and oligomerization has been demonstrated previously, for example, by Hantgan and González-Rodríguez.[16−18] However, these studies have exploited organic luminophores which are directly conjugated to the integrin rather than labeled integrin ligands.

RGD labeled probes have been extensively used in cancer research in optical and especially in the field of radiolabels.[19−22] The particular emphasis has been on targeting $\alpha_v\beta_3$ due to its overexpression on neo-endothelial and tumor cells. Indeed, recently Wang et al. described the application of a 5(6)-carboxyfluorescein-c(KRGDf) conjugate to a fluorescence polarization assay to quantify binding to integrin $\alpha_v\beta_3$.[23] RGD radiolabels have also been extensively applied to platelet biology for recognition aimed at imaging thrombi.[24]

By comparison, there have been relatively few luminescent probe-labeled RGD conjugates applied to the study of platelet integrin.[25] Furthermore, this contribution is, to our knowledge, the first report of an RGD labeled luminescent metal polypyridyl complex. We designed these probes with a view to their application in platelet biology as the ability to easily and

dx.doi.org/10.1021/bc5000737 | Bioconjugate Chem. 2014, 25, 928−944

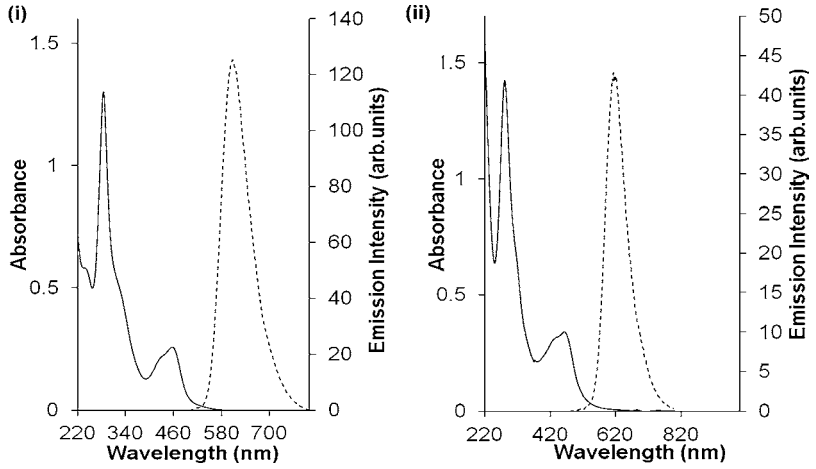

Figure 1. Absorption (continuous line) and emission (dashed line) spectra of (i) bpy-RGD (λ_{exc} 455) and (ii) dpp-RGD (λ_{exc} 465 nm). Concentration was 20 μM in acetonitrile in all cases.

Table 1. Summary of the Optical and Photophysical Properties of the Parent Complexes $[Ru(bpy)_2PIC]^{2+}$ and $[Ru(dpp)_2PIC]^{2+}$ and Dye–Peptide Conjugates, bpy-RGD and dpp-RGD[a]

			emission lifetime (μs)		
complex	absorbance (nm)/ε (mol^{-1} cm^{-1})	emission (nm)	aerated	deaerated	quantum yield
$[Ru(bpy)_2PIC]^{2+}$	457/13 033 ± 1473	608	0.16 ± 0.07	0.50 ± 0.05	0.068 ± 0.004
bpy-RGD	455/13 222 ± 1002	615	0.23 ± 0.03	0.58 ± 0.10	0.055 ± 0.002
			0.52 ± 0.04[b]	1.05 ± 0.15[b]	0.062 ± 0.003[b]
$[Ru(dpp)_2PIC]^{2+}$	462/17 681 ± 1263	607	0.20 ± 0.04	1.47 ± 0.12	0.020 ± 0.003
dpp-RGD	465/14 327 ± 1332	611	0.49 ± 0.07	2.30 ± 0.04	0.031 ± 0.002

[a]Absorbance and emission measurements were carried out in aerated acetonitrile (20 μM concentration). Quantum yields were carried out as described in ref 26 via measurements of the solution at five points between 0.02 and 0.1 absorbance in aerated media. [b]Carried out in PBS, pH 7.4 buffer solution.

quickly assess protein activation status or aggregation is of significant value in this field. Currently, determining integrin integrity and activation status requires expensive and time-consuming protocols such as SDS-PAGE and immunoprecipitation.[12,26]

Ru(II) polypyridyl complexes, because of their favorable optical and photophysical properties, are increasingly being applied in biological applications such as cell imaging[27] and as probes in the analysis of biodynamic processes.[28,29] Direct conjugation of ruthenium polypyridyl complexes to biomolecules such as proteins and peptides has been widely reported.[30−36] In particular, ruthenium complexes have been successfully applied in the area of DNA binding[31] leading to anticancer therapeutics[37−39] with, for example, two ruthenium anticancer drugs (NAMI-A and KP1019) successfully reaching clinical trial. Their polarized emissions and long emission decays make them particularly suited to time-resolved luminescence anisotropy studies, and in 1994, DeGraff et al. reported the first measurement of rotational correlation times for a series of ruthenium(II) complexes bound to macromolecular systems.[40] Since then, many groups have directly conjugated ruthenium complexes to protein.[33,41−47] However, although ruthenium has been fairly widely used in direct conjugation to proteins, and more recently to peptides,[48−50] ruthenium-peptide targets for the investigation of specific ligand interaction with proteins by luminescence anisotropy, have, to our knowledge, not yet been reported.

In this contribution, the synthesis of two novel luminescent peptide–metal conjugates is described: $[Ru(bpy)_2PIC\text{-}RGD]^{2+}$, bpy-RGD, and $[Ru(dpp)_2PIC\text{-}RGD]^{2+,}$ dpp-RGD, where dpp is 4,7-diphenyl-1,10-phenanthroline, bpy is 2,2′-bipyridine, and PIC is 2-(4-carboxyphenyl)imidazo[4,5*f*][1,10]phenanthroline, illustrated in Scheme 1. Both probes were conjugated using an active NHS ester terminus via an amide linkage to amino-hexanoic acid terminated RGD peptide, G-ahx-GRGDS. The application of these peptide complexes as molecular probes to report on integrin binding and activation status was investigated using steady state and time-resolved luminescence spectroscopy. Integrin, $\alpha_{IIb}\beta_3$, was treated with the ruthenium(II) polypyridyl RGD peptide conjugate, and the binding constant and the luminescence anisotropy compared before and after the integrin was treated with common "integrin activators", DTT and Mn^{2+}.

We found that the RGD conjugates showed both high affinity and specificity for $\alpha_{IIb}\beta_3$ in solution and that time-resolved luminescence anisotropy could be used to clearly distinguish between resting and integrin treated with Mn^{2+} or DTT. Live cell studies using confocal microscopy confirmed that these complex conjugates bind selectively to integrin at the cell membrane.

RESULTS

Photophysical Properties of bpy-RGD and dpp-RGD. The structures of the parent complexes and RGD peptide conjugates are shown in Scheme 1. The parent complexes, $[Ru(bpy)_2PIC]^{2+}$, (ii), and $[Ru(dpp)_2PIC]^{2+}$, (iii), were prepared and purified according to protocols reported previously in the case of $[Ru(bpy)_2PIC]^{2+}$ and for related analogues in the case of $[Ru(dpp)_2PIC]^{2+}$.[23−25] NMR, high

dx.doi.org/10.1021/bc5000737 | Bioconjugate Chem. 2014, 25, 928−944

resolution mass spectra, and HPLC were used to confirm structure and purity, respectively, of the resulting complexes (see Supporting Information).[23−25] The conjugation of the RGD peptide to each metal complex was conducted according to previously reported protocols.[51,52] This involved activating the carboxylic acid terminus toward NHS ester formation using the coupling reagent DCC (*N,N′*-dicyclohexylcarbodimide) to yield the $[Ru(bpy)_2PIC\text{-}NHS]^{2+}$ and $[Ru(dpp)_2PIC\text{-}NHS]^{2+}$ derivatives (photophysical data and high resolution mass spectra are presented in Supporting Information).[52] The active NHS esters reacted efficiently with the amine terminus of the glycine residue of the G-ahx-GRGDS peptide moiety, Scheme 1 (i), to yield the peptide conjugates, bpy-RGD, (iv), and dpp-RGD, (v), with 53% and 57% yields, respectively, following purification by silica column chromatography.

The absorbance and emission spectra of the bpy-RGD and dpp-RGD conjugates in acetonitrile are shown in Figure 1 (i) and (ii). For both $[Ru(bpy)_2PIC]^{2+}$ and $[Ru(dpp)_2PIC]^{2+}$, the optical properties of the parent complex, its NHS ester intermediate (Supporting Information), and the conjugate are very similar, reflected in the spectroscopic data presented in Table 1. As the peptide modification is relatively remote from the metal center, due to the amino-hexanoic acid linker, the similarity in optical properties is unsurprising and consistent with a previously reported peptide bound Ru(II) complex.[25] Bpy-RGD exhibits an absorbance centered at 455 nm (ε ~13 222 ± 1002 $mol^{-1}cm^{-1}$) attributed to the characteristic singlet metal to ligand charge transfer (MLCT) transition. An intense emission, attributed to ^{3}MLCT phosphorescence, is observed at 615 nm. The quantum yield (ϕ) and luminescence lifetime (τ) of bpy-RGD in aerated aqueous media are 0.055 ± 0.002 and 0.23 ± 0.03 μs, respectively. The bpy containing complexes, isolated as perchlorate salts, are hydrophilic and very water-soluble presenting a quantum yield (ϕ) and luminescence lifetime (τ) of 0.062 ± 0.003 and 0.52 ± 0.04 μs, respectively, in aerated PBS at pH 7.4. In deareated media the luminescence lifetime of bpy-RGD increases from 0.23 ± 0.03 μs to 0.58 ± 0.10 μs in acetonitrile and from 0.52 ± 0.04 μs to 1.05 ± 0.15 μs in PBS, pH 7.4.

Similarly, dpp-RGD exhibits an MLCT absorbance centered at 465 nm (ε ~14 327 ± 1332 $mol^{-1}cm^{-1}$) and intense ^{3}MLCT phosphorescence centered at 611 nm. The quantum yield (ϕ) and luminescence lifetime (τ) of dpp-RGD in aerated aqueous media (0.031 ± 0.002 and 0.49 ± 0.07 μs, respectively), as observed for bpy-RGD, are higher than those of the parent complex (ϕ = 0.020 ± 0.003 and 0.20 ± 0.04 μs, respectively). Similar increases in both lifetime and quantum yield have been observed previously for other metal complexes on conjugation of peptide and are attributed to weak exclusion of oxygen from the metal center by the peptide.[53] As expected, the dpp containing complexes are exceptionally oxygen sensitive and deaeration increases the lifetime from 0.49 ± 0.07 μs to 2.30 ± 0.04 μs.[54] The luminescent decays of both probes in aerated and deaerated environments are presented in Supporting Information.

The sensitivity of these complexes, particularly dpp-RGD, to O_2 is important as small changes in the O_2 accessibility of the metal center can cause large changes in luminescent lifetime and quantum yield which can be useful in reflecting protein binding. Furthermore, the exceptionally long lifetime of the peptide conjugates makes them suited to the study of rotational correlation times of high molecular weight proteins.

Bpy-RGD and dpp-RGD Integrin Binding Specificity: BSA Control. The effect of nonspecific protein binding on the emission intensity of the ruthenium RGD conjugates was assessed using bovine serum albumin, BSA, as a negative control since it does not contain a RGD recognition site (see Supporting Information). BSA dissolved in TrisHCl buffer (20 mM Tris-HCl, 150 mM NaCl, 1 mM $CaCl_2$, pH 7.4) was titrated into a solution of each ruthenium−peptide conjugate, to yield a final concentration of 1.1 μM of both complex and protein. The emission intensity of bpy-RGD or dpp-RGD increased modestly in the presence of BSA (λ_{exc} 450 nm) to a maximum of approximately 2-fold the initial emission intensity. As described, vide infra, the intensity changes elicited by nonspecific binding were much lower than those induced by $\alpha_{IIb}\beta_3$ binding. As reported for previous integrin ligand binding studies, all $\alpha_{IIb}\beta_3$ binding data presented in this report were corrected for nonspecific binding by subtracting the BSA/Ru emission intensity values from the $\alpha_{IIb}\beta_3$/Ru data.[55,56]

Bpy-RGD and dpp-RGD Binding to Resting $\alpha_{IIb}\beta_3$. Binding assays for bpy-RGD and dpp-RGD with $\alpha_{IIb}\beta_3$ were carried out using luminescence spectroscopy, monitoring at 610 nm. The resulting binding curves and associated spectra are presented in Figures 2 and 3 and their insets, respectively. The emission intensity increased significantly with increasing $\alpha_{IIb}\beta_3$ concentration, an effect attributed to changes to the complex's local microenvironment on protein binding, in particular, to

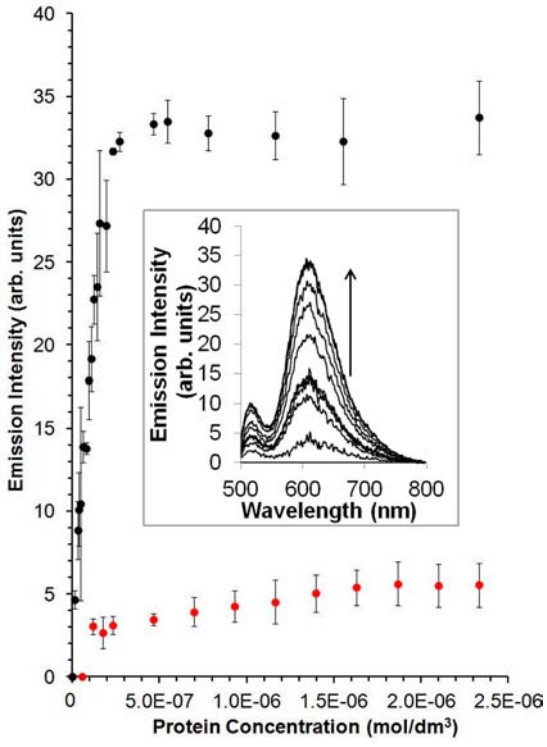

Figure 2. Luminescence titration of purified $\alpha_{IIb}\beta_3$ by bpy-RGD (black circle) and to BSA (red circle). Inset: Luminescence emission intensity changes (arb.units) of bpy-RGD following sequential addition of purified $\alpha_{IIb}\beta_3$. Corrections for dilution were inserted in all spectra recorded. Integrin $\alpha_{IIb}\beta_3$, dissolved in TrisHCl buffer (20 mM Tris-HCl, 150 mM NaCl, 1 mM $CaCl_2$, pH 7.4), was added sequentially to ruthenium-RGD in the same buffer, to yield a final concentration of 0.8 μM of both complex and protein. Stock concentration of bpy-RGD, BSA, and $\alpha_{IIb}\beta_3$ was 2.3 μM in TrisHCl buffer, pH 7.4, and bpy-RGD was held constant in all cases (λ_{exc} 450 nm, λ_{em} 610 nm).

dx.doi.org/10.1021/bc5000737 | *Bioconjugate Chem.* 2014, 25, 928−944

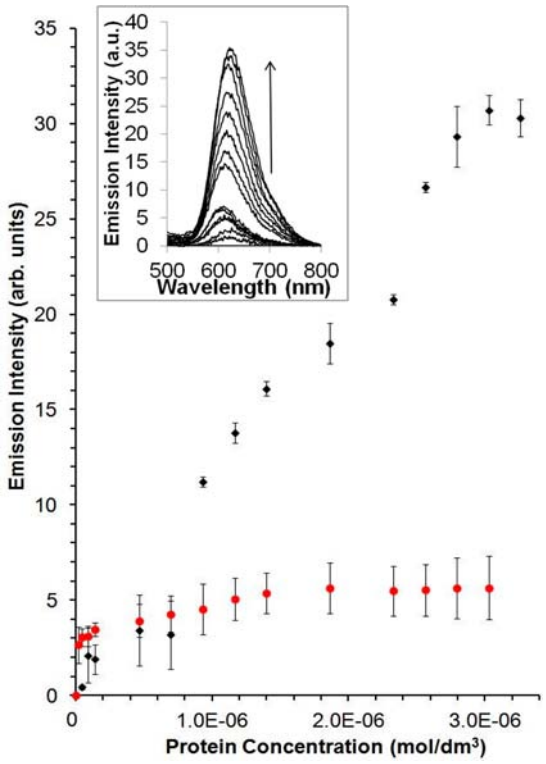

Figure 3. Luminescence titration of purified $\alpha_{IIb}\beta_3$ by dpp-RGD (black circle) and to BSA (red circle). Inset: Luminescence emission intensity changes (arb. units) of dpp-RGD following sequential addition of purified $\alpha_{IIb}\beta_3$. Corrections for dilution were inserted in all spectra recorded. Integrin $\alpha_{IIb}\beta_3$, dissolved in TrisHCl buffer (20 mM Tris-HCl, 150 mM NaCl, 1 mM $CaCl_2$, pH 7.4), was added sequentially to ruthenium-RGD in the same buffer, to yield a final concentration of 0.77 μM of both complex and protein. Stock concentration of dpp-RGD, BSA and $\alpha_{IIb}\beta_3$ was 2.3 μM in TrisHCl buffer, pH 7.4, and dpp-RGD was held constant in all cases. (λ_{exc} 450 nm, λ_{em} 610 nm).

inhibition of O_2 access to the ruthenium center. The absence of changes in the absorbance spectra of the complexes on binding is consistent with this (see Supporting Information). The binding of each probe to resting integrin is saturable and the final luminescence intensities of both bpy-RGD and dpp-RGD had increased by approximately an order of magnitude at saturation binding.

The dissociation constants (K_d) obtained by fitting the curves presented in Figures 2 and 3 are shown in Table 2. Bpy-RGD bound to a single site on the integrin protein with K_d = 0.09 ± 0.01 μM. Interestingly, the shape of the binding curve for $\alpha_{IIb}\beta_3$ titration against dpp-RGD (Figure 3) showed two plateaus which may be indicative of two-step binding, with an initial K_d = 0.25 ± 0.29 μM and second K_d = 4.37 ± 0.82 μM.

The luminescence decay times and time-resolved luminescence anisotropy of the ruthenium peptide conjugates bound to resting $\alpha_{IIb}\beta_3$ are also summarized in Table 2. An integrin/ruthenium ratio of 1.3:1 was used in all cases. For both metal conjugates, binding to $\alpha_{IIb}\beta_3$ led to an emission which decayed according to biexponential kinetics (see Supporting Information). The decays were dominated (>80% of amplitude) by a long-lived component, τ_1 > 1.1 μs, with the short-lived component τ_2 < 0.5 μs accounting for less than 20% of the amplitude attributed to unbound conjugate. The luminescent lifetime of bpy-RGD increased 2-fold to 1.10 ± 0.07 μs on integrin binding, compared to 0.52 ± 0.04 μs in the absence of integrin, whereas the lifetime of dpp-RGD increased 3-fold from 0.49 ± 0.07 μs to 1.43 ± 0.04 μs on integrin binding. These increases in lifetime are consistent with the increased emission intensity observed on association of each complex with $\alpha_{IIb}\beta_3$.

No luminescence anisotropy was observed for the ruthenium−peptide conjugates alone in solution, while binding to purified integrin $\alpha_{IIb}\beta_3$ induced luminescence anisotropy with a rotational correlation time of 1.50 ± 0.003 μs and 2.58 ± 0.04 μs for bpy-RGD and dpp-RGD, respectively. These rotational correlation times are consistent with values reported for other ruthenium(II) complexes directly conjugated to high molecular weight proteins, confirming binding of the RGD peptide probes to the integrin.[40,57] However, the difference in rotational correlation time between the two complexes is interesting and indicates that the metal complex binding directly affects protein structure. This is consistent with the

Table 2. Rotational Correlation Times, Luminescent Lifetimes, and Dissociation Constants of (left) bpy-RGD and (right) dpp-RGD in Absence of and Bound to $\alpha_{IIb}\beta_3$ as a Function of Its Chemical Treatment in TrisHCl buffer (pH 7.4) at RT from TCSPC (λ_{exc} 450 nm)[a]

	bpy-RGD			dpp-RGD		
integrin treatment	rotational correlation time (μs)	dissociation constant (K_D) ($\times 10^{-6}$)	luminescent lifetime[b] (μs)	rotational correlation time (μs)	dissociation constant (K_D) ($\times 10^{-6}$)	luminescent lifetime[b] (μs)
dye alone	–	-	0.52 ± 0.04	-	-	0.49 ± 0.07
resting $\alpha_{IIb}\beta_3$	1.50 ± 0.03	0.09 ± 0.01	1.10 ± 0.07	2.58 ± 0.04	0.25 ± 0.29, 4.37 ± 0.82	1.43 ± 0.04
postbind to $\alpha_{IIb}\beta_3$ (Mn^{2+})	1.29 ± 0.03	-	1.36 ± 0.05	1.72 ± 0.03	-	2.42 ± 0.04
pretreated $\alpha_{IIb}\beta_3$ (Mn^{2+})	1.12 ± 0.01	0.11 ± 0.01	1.21 ± 0.04	1.53 ± 0.04	0.17 ± 0.04	1.60 ± 0.13
postbind to $\alpha_{IIb}\beta_3$ (DTT)	1.04 ± 0.01	-	1.83 ± 0.07	1.29 ± 0.03	-	2.71 ± 0.04
pretreated $\alpha_{IIb}\beta_3$ (DTT)	0.59 ± 0.02	0.08 ± 0.01	1.20 ± 0.12	0.90 ± 0.02	0.15 ± 0.05	1.58 ± 0.07
bound to denatured $\alpha_{IIb}\beta_3$	0.46 ± 0.002	0.06 ± 0.01	1.16 ± 0.05	0.23 ± 0.04	1.35 ± 0.39	0.91 ± 0.09

[a]Anisotropy data was obtained from fit to eq 2, χ_r^2, reduced chi-square values were approximately 1 in all cases. Post-bind: Mn^{2+} or DTT was added after Ru-RGD was associated with resting $\alpha_{IIb}\beta_3$. Pre-treatment: Mn^{2+} or DTT was pre-incubated with $\alpha_{IIb}\beta_3$ prior to addition to Ru-RGD. Denatured: $\alpha_{IIb}\beta_3$ was denatured for 1 h at 90 °C prior to incubation with Ru-RGD. The stock concentration of Ru-RGD and $\alpha_{IIb}\beta_3$ was 2.3 μM. Mn^{2+} and DTT were added at a 10:1 ($\alpha_{IIb}\beta_3$: Ru-RGD) ratio. Ru-RGD concentration was held constant in all cases. [b]In aerated media.

dx.doi.org/10.1021/bc5000737 | Bioconjugate Chem. 2014, 25, 928−944

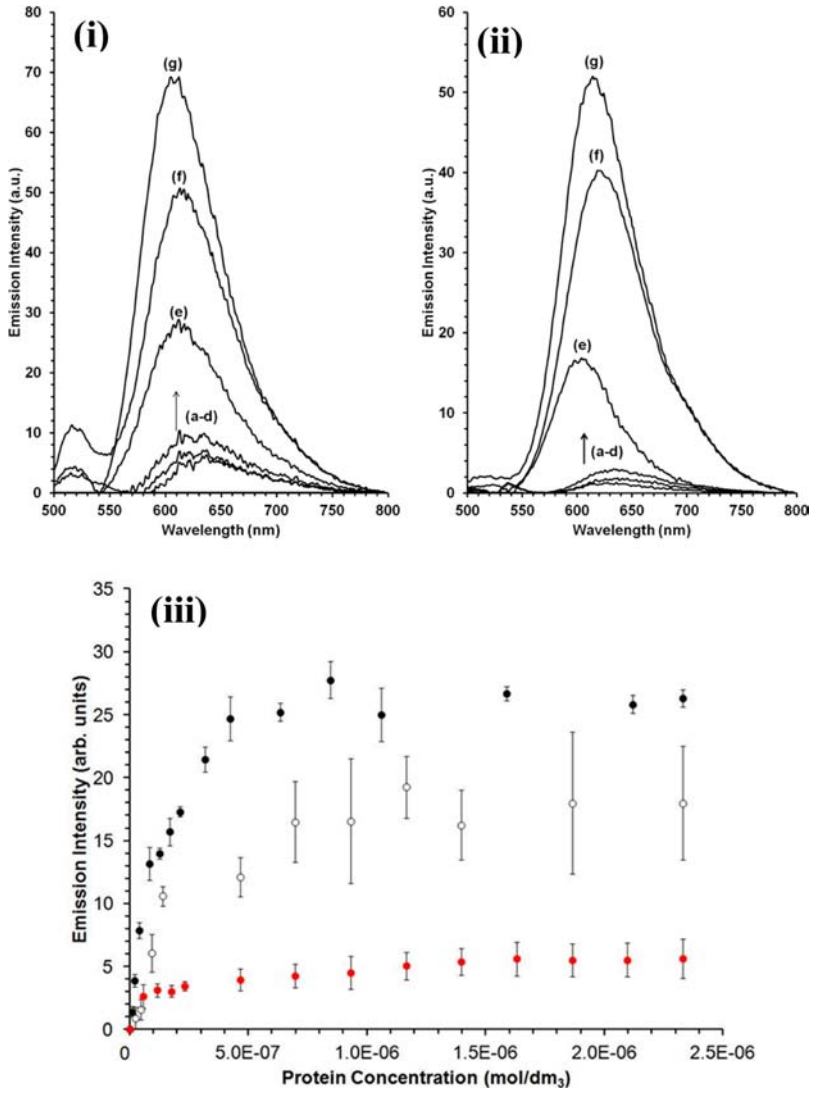

Figure 4. Effect of Mn^{2+} chemical treatment of $\alpha_{IIb}\beta_3$ on the luminescence spectroscopy of bound (i) bpy-RGD or bound (ii) dpp-RGD where bpy-RGD or dpp-RGD is incubated (a) alone in solution, (b) with Mn^{2+}, (c) with BSA, (d) with BSA and Mn^{2+}, (e) with $\alpha_{IIb}\beta_3$ pretreated with Mn^{2+}, (f) with untreated $\alpha_{IIb}\beta_3$, or (g) Mn^{2+} postbinding the dye probe to untreated $\alpha_{IIb}\beta_3$. (iii) Bpy-RGD (black circle) and dpp-RGD (white circle) emission intensity changes following binding to integrin pretreated with Mn^{2+} and corrected for nonspecific binding with BSA (red circle). The $\alpha_{IIb}\beta_3$/ruthenium-RGD ratio was 1:1. The stock concentration of bpy-RGD, dpp-RGD, $\alpha_{IIb}\beta_3$, and BSA was 2.3 μM in TrisHCl buffer pH 7.4 for all experiments. Mn^{2+} concentration was 23 μM (10:1 Mn^{2+}:$\alpha_{IIb}\beta_3$ ratio). Bpy-RGD and dpp-RGD concentration was held constant in all cases. (λ_{ex} 450, λ_{em} 610 nm, and slit width of 10 nm.)

differences observed in the binding curves. The rotational correlation time particularly for the dpp-RGD integrin complex is longer than expected on the basis of the molecular weight of the integrin (approximately 240 kDa). This may indicate that RGD-conjugate binding induces oligomerization of $\alpha_{IIb}\beta_3$ (note: low integrin concentrations were used in these studies to avoid aggregation of the integrin and DLS and SDS page confirmed little aggregation of the $\alpha_{IIb}\beta_3$ in the protein samples prepared for these studies; therefore, we conclude that if aggregation is occurring it is being induced by RGD conjugates). Such behavior has been reported previously for $\alpha_{IIb}\beta_3$ in solution where a range of RGD peptides were found to induce self-association.[58,59]

Bpy-RGD and dpp-RGD Binding Specificity: Eptifibatide. To determine if bpy-RGD and dpp-RGD bind specifically at the RGD binding motif on $\alpha_{IIb}\beta_3$, a displacement experiment was carried out using Eptifibatide. Eptifibatide is a glycoprotein integrin $\alpha_{IIb}\beta_3$ inhibitor which binds at the RGD binding motif with a K_d in the nM range compared to the μM range indicated for the ruthenium-peptide probes discussed here.[60−63] As its binding affinity for $\alpha_{IIb}\beta_3$ is 2 to 3 orders of magnitude greater than bpy-RGD or dpp-RGD, it was expected that Eptifibatide would effectively compete for the RGD recognition site and prevent metal complex binding. The effect of sequential addition of $\alpha_{IIb}\beta_3$ to a solution containing a 1:1 molar ratio of Eptifibatide:bpy-RGD or Eptifibatide:dpp-RGD on the emission intensities of the ruthenium centers is presented in Supporting Information. In both cases only minor increases in emission intensity of the ruthenium complex were observed, which were comparable in magnitude to the intensity changes observed on nonspecific binding to BSA.

In addition, the effect of sequential addition of $\alpha_{IIb}\beta_3$ to each of the metal complexes (bpy-RGD or dpp-RGD), where the integrin has first been incubated with Eptifibatide (1:1 molar ratio) is presented in Supporting Information. Similarly, only

dx.doi.org/10.1021/bc5000737 | Bioconjugate Chem. 2014, 25, 928−944

modest intensity increases are observed consistent with nonspecific interactions only.

As Eptifibatide is specific for the RGD binding site, these results indicate that its presence inhibits bpy-RGD and dpp-RGD binding to $\alpha_{IIb}\beta_3$ confirming that both complexes bind specifically to the RGD recognition site.

The Influence of Chemical Activation of $\alpha_{IIb}\beta_3$ on Its Interaction with bpy-RGD and dpp-RGD. Although "inside-out" $\alpha_{IIb}\beta_3$ activation *in vivo* is normally regulated by agonist-generated signaling, $\alpha_{IIb}\beta_3$ can also be activated by a range of chemical stimuli including Mn^{2+} and DTT.[13,64] Thus, to assess the capacity of bpy-RGD and dpp-RGD to discriminate between chemically activated and resting integrin, the influence of treatment of the integrin with Mn^{2+} or DTT on ruthenium-RGD binding were explored.

The Influence of Mn^{2+} Chemical Activation of $\alpha_{IIb}\beta_3$ on Its Interaction with bpy-RGD and dpp-RGD. $\alpha_{IIb}\beta_3$ is composed of two noncovalently associated subunits, GPIIB (α_{IIb}) and GPIIIa (β_3), and divalent cations Ca^{2+} and Mg^{2+} stabilize association of these subunits. Integrins contain multiple cation binding sites that influence its ligand binding affinity as well as activation state. All of the regions implicated in ligand recognition lie at, or close to, cation-binding sites, and ligand binding and cation binding are intimately linked.[65−67]

It has been shown that Mn^{2+} directly modulates the binding activity of integrins to fibrinogen, fibronectin, and RGD peptide mimetics.[67−69] For example in 2002, Takagi et al. reported a conformational change in the crystal structure of the extracellular domain of $\alpha_V\beta_3$ to a bent conformation in the presence of Ca^{2+} and to an extended conformation in the presence of Mn^{2+}, giving rise to the "switchblade" hypothesis (the extended conformation of $\alpha_V\beta_3$ represents the active state and the bent shape represents the resting state).[70] However, it appears to be unable to maintain the active-like state, which led to the suggestion by Arnaut et al. that a cofactor is required such as an RGD ligand.[71] Their crystallographic studies indicated that even at very high relative concentrations of Mn^{2+} the conformation at the extracellular portion of a related integrin $\alpha_V\beta$ remained relatively unchanged from its resting state except in the presence of a high-affinity RGD ligand.[66] However, Weisel and co-workers have shown that Mn^{2+} increases integrin affinity for and kinetics of binding to its primary ligand fibrinogen.[69]

The emission spectra of bpy-RGD and dpp-RGD following 10 min (note: longer incubation times did not change the spectral data) incubation with integrin ($\alpha_{IIb}\beta_3$/ruthenium-RGD ratio was 1:1) before and after treatment of the integrin with Mn^{2+} are shown in Figure 4 (i) and (ii). In these experiments Mn^{2+} was present in 10-fold excess to integrin. The emission data shown in Figure 4 are absorption matched (see Supporting Information), so that the emission intensity can be quantitatively compared.

Figure 4 (i) and (ii) (a−d) shows the emission spectra of the ruthenium-RGD conjugate alone in PBS solution without and with Mn^{2+}, and confirms that Mn^{2+} does not directly affect the photophysics of the metal complexes. Similarly, the metal complex conjugates in the presence of BSA and in the presence of BSA and Mn^{2+} do not show any change in emission intensity when Mn^{2+} is present. In contrast, treatment of bpy-RGD bound to resting $\alpha_{IIb}\beta_3$ with Mn^{2+} caused a significant increase (∼50%) in the emission quantum yield of the ruthenium conjugate, Figure 4 (i), (g). However, interestingly, where the conjugate probe bpy-RGD was bound to the $\alpha_{IIb}\beta_3$ after the integrin had been first incubated with Mn^{2+}, Figure 4 (i) (e), the emission intensity of bpy-RGD was lower by 21% than the conjugate bound to resting integrin.

The behavior was analogous for dpp-RGD. Treatment of resting integrin with Mn^{2+} after the dpp-RGD had been previously incubated with $\alpha_{IIb}\beta_3$ caused an increase (∼23%) in the emission quantum yield of the ruthenium conjugate (Figure 4 (ii), (g)), whereas pretreatment of the integrin with Mn^{2+} before binding to the ruthenium probe Figure 4 (ii) (e) reduced the emission of the integrin bound probe by ∼40% compared with the dpp-RGD bound to the resting (untreated) integrin.

To quantify the effect of Mn^{2+} treatment of $\alpha_{IIb}\beta_3$ binding to the ruthenium conjugates, the binding curves were obtained for each metal complex with the Mn^{2+} treated integrin, shown in Figure 4 (iii). For bpy-RGD titrated with the Mn^{2+} treated integrin, a K_d of 0.11 ± 0.01 μM was obtained, suggesting that bpy-RGD binds to a single site and that K_d is unchanged from the native $\alpha_{IIb}\beta_3$ (Table 2).

In contrast, pretreatment of the integrin with Mn^{2+} had a dramatic effect on the binding of dpp-RGD to the protein. As shown in Figure 4 (iii), the binding curve, which for the resting integrin was a two-step process, becomes a single-step binding process, following integrin treatment with Mn^{2+}. K_d was determined to be 0.17 ± 0.04 μM, suggesting that dpp-RGD binds to a single site, and unlike bpy-RGD, the binding constant is smaller for the Mn^{2+} treated $\alpha_{IIb}\beta_3$, indicating that the complex has higher affinity for the integrin protein following Mn^{2+} treatment (see Table 2).

These results show, rather surprisingly, that the affinity of bpy-RGD for Mn^{2+} treated integrin is the same as resting integrin, but that binding affinity of dpp-RGD for Mn^{2+} treated integrin is increased compared to resting. This suggests that the counter ligand (e.g., bpy versus dpp) plays a role in the interaction of the metal complex RGD conjugate with integrin. The differences in affinity of the two complexes for the resting integrin and the two-step binding curve observed for the resting integrin for dpp-RGD also concur with this observation. It is noteworthy, however, that as indicated by the Eptifibatide studies described above, both complexes recognize the RGD binding site.

The key differences between bpy-RGD and dpp-RGD are their size and, particularly, hydrophobicity. The dpp complex (molecular weight: 1748.62 g/mol) is expected to be approx 25% larger and considerably more hydrophobic than the bpy complex (molecular weight: 1397.24 g/mol). In addition, the perchlorate salt of the parent complex dpp-RGD is not water-soluble, whereas the bpy complex is.

Based on the two-step binding to the resting integrin it is tempting to speculate that both RGD binding and hydrophobic−hydrophobic interactions occur for dpp-RGD and that the larger size of this complex prevents deep penetration of the complex into the RGD binding pocket, which may account for the increased affinity observed for RGD binding to the Mn^{2+} activated protein. For bpy-RGD, the K_d with the integrin is the same before and after Mn^{2+} treatment and the association constant to the resting integrin is greater than dpp-RGD. This suggests that this complex is more accessible to the RGD binding site and is in good agreement with previously reported small peptide mimetic binders.[72−75]

Interestingly, addition of Mn^{2+} whether before or after integrin binding to the metal complex conjugate had a similar impact on the rotational correlation time of the Ru(II) probes

dx.doi.org/10.1021/bc5000737 | Bioconjugate Chem. 2014, 25, 928−944

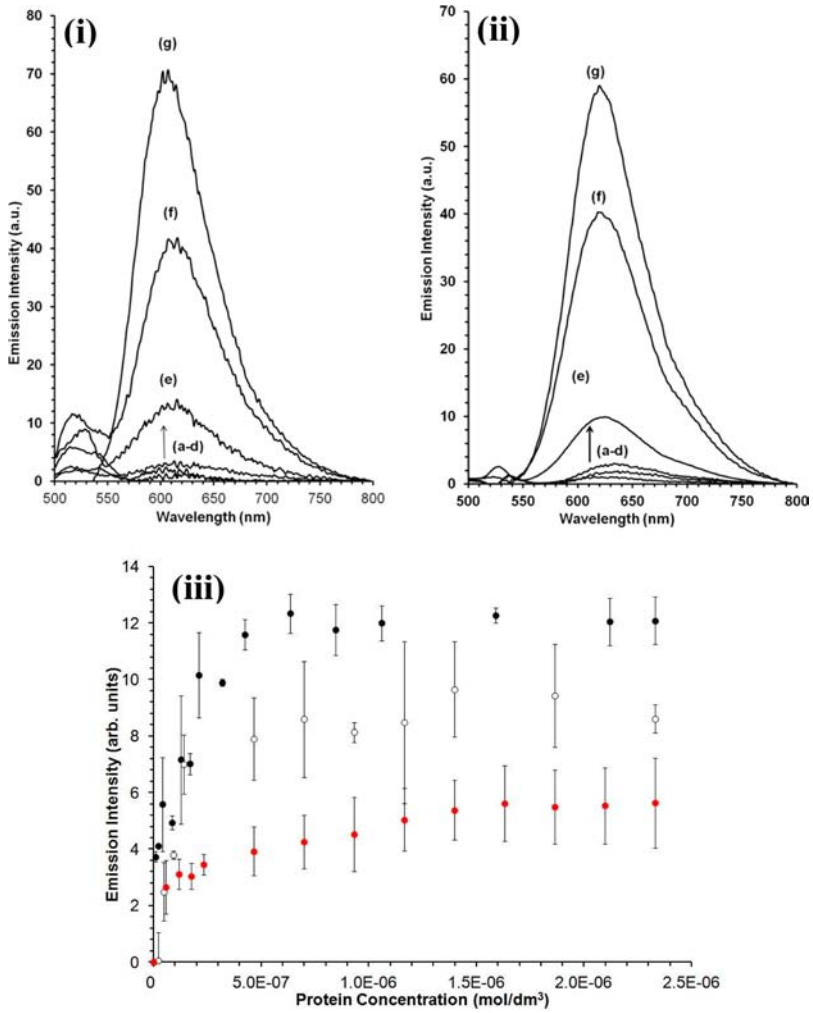

Figure 5. Effect of DTT chemical treatment of $\alpha_{IIb}\beta_3$ on the luminescence spectroscopy of bound (i) bpy-RGD or bound (ii) dpp-RGD where bpy-RGD or dpp-RGD is incubated (a) alone in solution, (b) with DTT, (c) with BSA, (d) with BSA and DTT, (e) with $\alpha_{IIb}\beta_3$ pretreated with DTT, (f) with untreated $\alpha_{IIb}\beta_3$, and (g) DTT postbinding the dye probe to untreated $\alpha_{IIb}\beta_3$. (iii) bpy-RGD (black circle) and dpp-RGD (white circle) emission intensity changes following binding to integrin pretreated with DTT and corrected for nonspecific binding with BSA (red circle). The $\alpha_{IIb}\beta_3$/ruthenium-RGD ratio was 1:1. The stock concentration of bpy-RGD, dpp-RGD, $\alpha_{IIb}\beta_3$, and BSA was 2.3 μM in TrisHCl buffer pH 7.4 for all experiments. DTT concentration was 23 μM (10:1 DTT:$\alpha_{IIb}\beta_3$ ratio). Bpy-RGD and dpp-RGD concentration was held constant in all cases. (λ_{ex} 450, λ_{em} 610 nm, and slit width of 10 nm).

once bound. This data is captured in Table 2. Bpy-RGD showed a decrease in rotational correlation time from 1.50 ± 0.03 μs (resting integrin) to 1.29 ± 0.03 μs following the addition of Mn^{2+} to the Ru(II)-integrin complex. The rotational correlation time for bpy-RGD when bound to integrin which had been previously incubated with Mn^{2+} was recorded as 1.12 ± 0.01 μs, i.e., the reduction in rotational correlation time was greater when the integrin was treated with activator prior to probe binding. Similarly, dpp-RGD exhibited a decrease in rotational correlation time from 2.58 ± 0.04 μs (resting integrin) to 1.72 ± 0.03 μs following the addition of Mn^{2+} to the integrin−probe complex but was lower again at 1.53 ± 0.04 μs when the integrin was treated with Mn^{2+} prior to the Ru(II) probe binding.

Therefore, both peptide probes recorded the conformational change in the integrin induced by the Mn^{2+}, but interestingly, preassociation of each of the complexes with the integrin influences the final conformational state the integrin attains. This may also indicate that integrin self-association induced by the RGD ligand is modulated by Mn^{2+} treatment.

In contrast, activation of integrin with Mn^{2+} exerts an influence on the luminescent lifetime of bpy-RGD or dpp-RGD, only if the metal complex conjugate is bound to the integrin prior to its activation. If the $\alpha_{IIb}\beta_3$ is pretreated with Mn^{2+} prior to binding to bpy-RGD, there is, within experimental error, no change to the luminescent lifetime of the probe; 1.10 ± 0.07 μs (resting) versus 1.21 ± 0.04 μs (Mn^{2+}) (Table 2). In contrast, if the complex is already bound to the integrin prior to Mn^{2+} treatment, the lifetime of the probe is found to increase to 1.36 ± 0.05 μs (Table 2).

Similarly, if the $\alpha_{IIb}\beta_3$ is treated with Mn^{2+} prior to its exposure to dpp-RGD, there is, within experimental error, no change to the luminescent lifetime of the probe: 1.43 ± 0.04 μs (resting) compared to 1.60 ± 0.13 μs (Mn^{2+}) (Table 2), whereas when the probe is already bound to the integrin and then treated with Mn^{2+}, the lifetime of the probe increased dramatically, to 2.42 ± 0.04 μs (Table 2).

The increase in lifetime of the prebound probe in each instance correlates with the observed increase in emission

dx.doi.org/10.1021/bc5000737 | Bioconjugate Chem. 2014, 25, 928−944

intensity of the final complex following chemical treatment post association to integrin, as shown in Figure 4, (ii), (g).

The Influence of DTT Chemical Activation of $\alpha_{IIb}\beta_3$ on Its Interaction with bpy-RGD and dpp-RGD. DTT is a powerful reducing agent, because its oxidized product is stabilized by a six-membered ring with an internal disulfide bond. The requirement of specific cysteine−cysteine disulfide bonds for the maintenance of integrin activation is well reported.[13,76,77] Treatment of platelets or integrin with DTT has been shown to increase the ligand binding affinity of the integrin,[13,78] attributed to the formation of an active conformation of the protein stimulated by disulfide reduction.[79]

The effects of DTT treatment of $\alpha_{IIb}\beta_3$ on the emission of dpp-RGD or bpy-RGD binding to the integrin are shown in Figure 5 (i) and (ii). In all cases, DTT was added in 10-fold molar excess to the integrin. The emission spectra were recorded following 10 min incubation of the integrin−probe complex with DTT (longer incubation times did not change the spectral data).

Figure 5 (i) and (ii) (a−d) presents the control experiments where the emission spectra of each metal complex conjugate were recorded in the absence of $\alpha_{IIb}\beta_3$: alone with DTT, in the presence of BSA, and in the presence of BSA and DTT. No relative change in emission intensity was observed, indicating that DTT has no direct effect on the photophysics of the ruthenium conjugate.

Incubation of the bpy-RGD:$\alpha_{IIb}\beta_3$ complex with DTT results in a significant increase (~58%) in the emission quantum yield of the ruthenium conjugate (Figure 5 (i) (g)). Conversely, when $\alpha_{IIb}\beta_3$ was incubated with DTT prior to binding to bpy-RGD (Figure 5 (i) (e)), the final integrated emission intensity of bpy-RGD once bound to the integrin was reduced by ~30% compared to resting integrin; however, this difference may arise due to the lower binding constant (Table 2). Similarly, after dpp-RGD had been incubated first with the resting integrin (Figure 5 (ii) (f)), the addition of DTT caused a significant increase (~31%) in the emission quantum yield of the protein bound ruthenium conjugate (Figure 5 (ii) (g)), whereas the final integrated emission intensity of dpp-RGD was reduced by ~80% compared to resting integrin when $\alpha_{IIb}\beta_3$ was treated with DTT prior to its association with dpp-RGD (Figure 5 (ii) (e)).

Overall, although the magnitude of the emission intensity changes induced by DTT are greater, the trend is the same as for Mn^{2+} treatment and suggests again that prebinding of either ruthenium peptide conjugate to $\alpha_{IIb}\beta_3$ influences the final conformation the integrin achieves following activator treatment.

Figure 5 (iii) shows the binding curve for bpy-RGD with DTT treated $\alpha_{IIb}\beta_3$. The sigmoidal curve indicates single site binding and K_d was determined to be 0.08 ± 0.01 μM, comparable to the K_d determined for resting and DTT treated $\alpha_{IIb}\beta_3$ (Table 2). For dpp-RGD, as seen following treatment with Mn^{2+}, the binding curve for this complex with the DTT treated integrin changed from the two-step curve seen for the resting integrin to a single-step binding curve (Figure 5 (iii)). K_d was estimated to be 0.15 ± 0.05 μM (Table 2), indicating that dpp-RGD binds to a single site with higher affinity compared to the two-step binding to resting $\alpha_{IIb}\beta_3$ (Figure 3).

Addition of DTT both prior to or after bpy-RGD association with the integrin $\alpha_{IIb}\beta_3$ resulted in significant decreases in the rotational correlation time of the Ru(II) center (Table 2). The rotational correlation time for the metal complex was 1.04 ± 0.01 μs following DTT treatment of the Ru:integrin complex (a 14% decrease compared to resting integrin), and this was reduced further to 0.59 ± 0.02 μs if $\alpha_{IIb}\beta_3$ was exposed to DTT prior to its association with bpy-RGD (61% decrease compared to resting integrin).

For dpp-RGD the rotational correlation time of this complex was found to be 1.29 ± 0.03 μs when DTT was applied to the Ru:integrin complex (a 50% decrease compared to resting integrin), and this was reduced further to 0.90 ± 0.02 μs if $\alpha_{IIb}\beta_3$ was exposed to DTT prior to its association with dpp-RGD (65% decrease compared to resting integrin) (Table 2). The magnitude of the decrease in rotational time was constant with activator treatment.

Consistent with the behavior observed for Mn^{2+} induced activation, treating integrin with DTT only had a significant effect on the luminescence lifetime of the Ru-RGD compounds if the probe was bound to the integrin prior to its activation (Table 2). The luminescent lifetime of bpy-RGD increased to 1.83 ± 0.07 μs following DTT treatment of the integrin. Similarly, the lifetime of dpp-RGD was found to increase to 2.72 ± 0.04 μs for DTT treated integrin (Table 2). The increased lifetime for each probe bound to the integrin following DTT treatment correlates well with increased emission intensity observed for the integrin-probe complexes on DTT treatment (Figure 4 (i) and (ii), (f)).

That both lifetime and time-resolved luminescence anisotropy change in response to Mn^{2+} or DTT treatment of the probe−integrin complex indicates that a conformational change has been induced in the complex by the activator. That there is a difference in the emission lifetime of the probe depending on whether it was in place when the integrin was treated with the activator or not indicates that its presence influences the final conformation or state of self-association of the integrin achieved and this state differs depending on Mn^{2+} or DTT activation. This difference may originate from oligomerization of the integrin induced by dpp-RGD or bpy-RGD where they are bound to the integrin prior to its activation.

The Influence of Denaturing $\alpha_{IIb}\beta_3$ on Its Interaction with bpy-RGD and dpp-RGD. As denaturation of $\alpha_{IIb}\beta_3$ will induce gross structural change in the protein, we examined the effect of denaturation on probe binding and photophysics by incubating the integrin at 90 °C for 1 h prior to binding to the peptide conjugates. We rationalized that by comparing the changes induced by denaturing $\alpha_{IIb}\beta_3$ on probe binding and photophysics we could benchmark somewhat the extent of conformational change induced with DTT and Mn^{2+}. The emission spectra of bpy-RGD and dpp-RGD following incubation with denatured integrin ($\alpha_{IIb}\beta_3$/ruthenium-RGD ratio was 1:1) are shown in Supporting Information. The binding curves for each peptide probes with $\alpha_{IIb}\beta_3$ are shown in Figure 6 (i) and (ii), and show that both exhibit saturable binding to the denatured integrin.

Interestingly, both metal peptide conjugates associated strongly with the denatured integrin and showed significant increases in emission intensity and lifetime on binding compared with the free complex (Table 2). A K_d of 0.06 ± 0.01 μM was obtained for bpy-RGD with denatured integrin, indicating a slightly higher binding affinity than $\alpha_{IIb}\beta_3$ treated with either DTT or Mn^{2+} (Table 2 and Figure 6 (i)). The emission quantum yield of the denatured integrin:bpy-RGD increased by ~44% compared to the complex bound to resting $\alpha_{IIb}\beta_3$, but within experimental error, the lifetime was unchanged. As expected, denaturing the protein resulted in a

dx.doi.org/10.1021/bc5000737 | Bioconjugate Chem. 2014, 25, 928−944

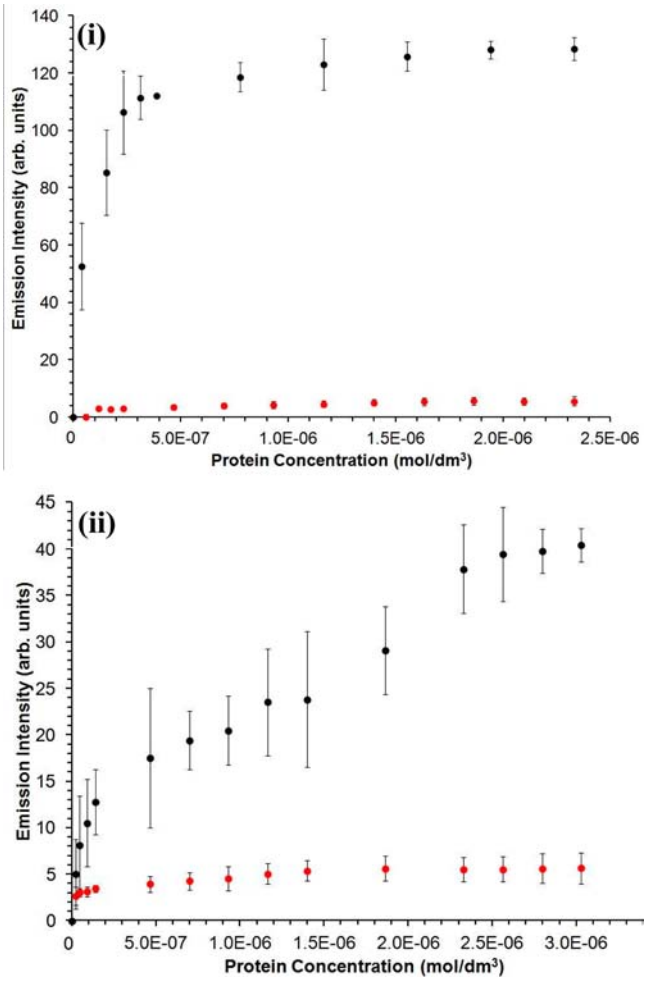

Figure 6. Binding curve for (i) dpp-RGD and (ii) bpy-RGD with denatured $\alpha_{IIb}\beta_3$ (black circle) and BSA (red circle). $\alpha_{IIb}\beta_3$ was denatured prior to the titrations by incubation at 90 °C for 1 h. The emission intensity data presented is corrected for contributions to nonspecific binding with BSA. In all cases, the stock concentration of bpy-RGD, dpp-RGD, and $\alpha_{IIb}\beta_3$ was 2.3 μM in TrisHCl buffer pH 7.4. In all cases, bpy-RGD and dpp-RGD were held constant. (λ_{ex} 450, λ_{em} 610 nm, and slit width of 10 nm).

large decrease in rotational correlation time of the Ru(II) center presenting a value of 0.46 ± 0.002 μs (roughly 3 times faster than that of the probe bound to the resting integrin; Table 2). For dpp-RGD the quantum yield of the complex bound to denatured integrin also increased, by ~30%, compared to resting $\alpha_{IIb}\beta_3$ and a K_d value of 1.35 ± 0.39 μM was obtained, indicating a lower binding affinity than $\alpha_{IIb}\beta_3$ treated with either DTT or Mn^{2+} (Table 2 and Figure 6 (ii)).

As for the bpy complex, the rotational correlation time of the dpp-RGD center decreased dramatically on binding to the denatured protein to 0.23 ± 0.04 μs (resting integrin; Table 2). Binding of the probe to the denatured integrin concomitantly decreased the lifetime of the probe to 0.91 ± 0.09 μs compared with 1.43 ± 0.04 for the probe bound to resting integrin. The very large reduction in rotational time constant observed for both dpp-RGD and bpy-RGD on binding to denatured integrin compared with resting or indeed Mn^{2+} or DTT activated integrin is consistent with extensive disruption of protein secondary and tertiary structure expected on heat treatment. The magnitude of the difference in rotational correlation time between the denatured and intact resting integrin is also suggestive that self-association of $\alpha_{IIb}\beta_3$ is induced by the dpp-RGD or bpy-RGD on binding to the resting integrin.

The greater influence of denaturation on the lifetime of dpp-RGD compared to bpy-RGD is attributed to the greater oxygen sensitivity of the former probe. The exposure afforded by loss of the RGD binding pocket in the intact protein leads to a greater reduction in its luminescence lifetime. Comparison of the rotational correlation times for the probes bound to Mn^{2+} and DTT treated integrin compared to denatured integrin confirms that these treatments do not denature the integrin and these probes through their luminescence anisotropy provide useful markers for the extent of conformational change and oligomerizaion in the integrin.

Cell Uptake and Localization of bpy-RGD and dpp-RGD. As bpy-RGD and dpp-RGD present strong and specific binding to the integrin and can report, based on luminescence anisotropy, lifetime and binding constant, on the conformational status of the protein, we were interested to see if the complex conjugates can bind to resting integrin within live cells. Two types of Chinese hamster ovary (CHO) cells were used in this study: wild type, CHO-WT cells not expressing $\alpha_{IIb}\beta_3$ and transfected CHO-$\alpha_{IIb}\beta_3$ cells expressing the resting form of $\alpha_{IIb}\beta_3$. Minimal staining of either cell type was observed when, in a control experiment, the cells were incubated with either parent complex: $[Ru(bpy)_2PIC]^{2+}$ or $[Ru(dpp)_2PIC]^{2+}$ (Supporting Information). Similarly the peptide conjugates, bpy-RGD or dpp-RGD, exhibited only weak staining of the CHO-WT cells, i.e., when there is no $\alpha_{IIb}\beta_3$ expression (Supporting Information). The wild type CHO expresses $\alpha_V\beta_1$, which may bind RGD, but is present at low abundance in these cells.[80,81]

In contrast, when CHO-$\alpha_{IIb}\beta_3$ expressing the resting form of $\alpha_{IIb}\beta_3$ was incubated with the bpy-RGD or dpp-RGD peptide conjugates, the cells showed extensive staining reflected in an intense ruthenium based emission. The emission maximum was confirmed to be at 610 nm, using a Zeiss Meta Microscope. The emission was shown to be localized at the cell surface, confirmed by *z*-stack imaging (Supporting Information), suggesting binding to the cell-surface integrin receptor. To confirm this was the case, the cells were incubated with bpy-RGD or dpp-RGD and co-labeled with SZ22, an α_{IIb} specific antibody. In both cases the metal complex conjugate co-localized strongly at the cell surface, with the integrin specific antibody as shown in Figure 7 (a) and (b), respectively. A total of ~48% integrin expression was determined from flow cytometry (see Supporting Information); correspondingly, ~52% of the CHO-$\alpha_{IIb}\beta_3$ cells within the culture do not express the integrin, and it was confirmed that, where a cell does not express integrin, it did not bind to either ruthenium-RGD probe and was also not stained by SZ22. A larger area image presenting multiple CHO cells both expressing and not expressing integrin $\alpha_{IIb}\beta_3$ are shown in the Supporting Information.

DISCUSSION

Both bpy-RGD and dpp-RGD bind with reasonably high affinity to resting integrin $\alpha_{IIb}\beta_3$. Contrasting evidence regarding the ability of RGD to bind to resting integrin/platelets has been reported.[72,74] Binding of fibrinogen to resting platelets is negligible and is tightly regulated by activation of platelets through various forms of stimuli (ADP, thrombin, etc.).[74] However, small RGD peptide mimetics have been found to bind with equally high affinity to both resting and

dx.doi.org/10.1021/bc5000737 | *Bioconjugate Chem.* 2014, 25, 928−944

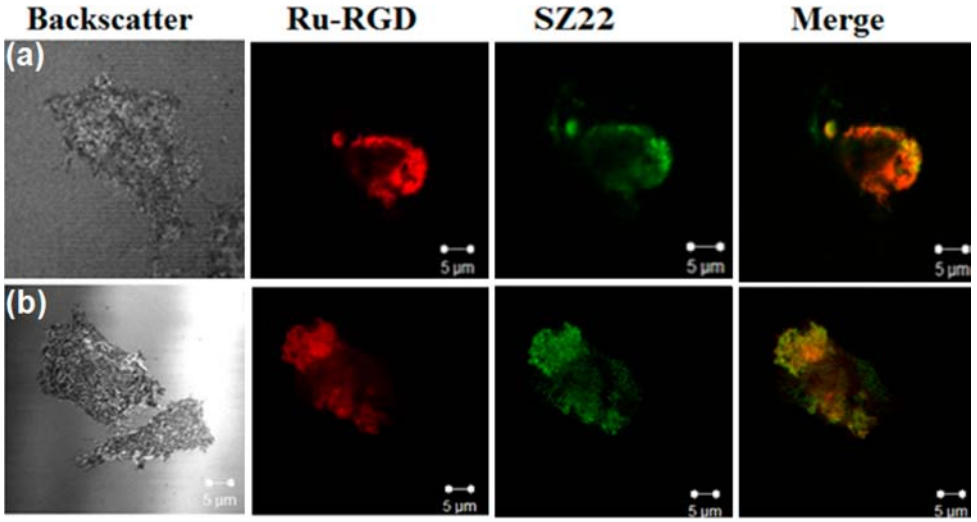

Figure 7. Luminescence confocal image of a transfected CHO-$\alpha_{IIb}\beta_3$ cell expressing the resting form of integrin $\alpha_{IIb}\beta_3$ compared to a CHO cell not expressing the integrin protein in the same image. In contrast to the controls presented in the Supporting Information, (a) bpy-RGD and (b) dpp-RGD, Ru-RGD (red) successfully co-localized with SZ22 (green) localizing on the surface of the cell (merge, yellow). Ru-RGD was added at 70 μM concentration in PBS (pH 7.4) and incubated at 37 °C for 4 h. SZ22 was added 1/250 dilution overnight at 4 °C and secondary AlexaFluor488 goat anti-mouse was added 1/500 for 2 h at room temperature. Excited at 458 nm, ruthenium luminescence was collected with a long pass filter of 615 nm. No luminescence is observed on the cell failing to express the integrin protein.

activated integrin and platelets.[72] For example, Echistatin, which contains an RGD sequence, binds with high affinity to resting and activated platelets.[73] Hu et al.[74] suggest that two ligand binding pockets exist within integrin $\alpha_{IIb}\beta_3$: one which binds RGD type ligands and the other which binds to fibrinogen. In this latter study, the binding ability of both fibrinogen and Fab-9 (a human antibody engineered by phage display to contain an RGD in the antigen binding site) to resting versus activated platelets was investigated. Fab-9 bound with equal affinity to both resting and activated platelets, whereas in contrast, fibrinogen bound solely to activated platelets. Further investigations confirm that the binding sites for RGD ligands and fibrinogen are spatially distinct yet coupled allosterically. Thus, RGD peptide mimetics seem to have the ability to bind to the β_3 subunit of both resting and activated forms of integrin $\alpha_{IIb}\beta_3$ and platelets.

The results presented here are consistent with this picture, which indicate that both bpy-RGD and dpp-RGD bind to both resting and activated $\alpha_{IIb}\beta_3$ in solution with comparable affinity. The specificity of both complexes toward the RGD binding pocket was confirmed since Eptifibatide, a cyclic RGD with higher binding affinity for this site prevented each complex from binding to $\alpha_{IIb}\beta_3$. Bpy-RGD exhibited lower K_d values than dpp-RGD, particularly for resting integrin, indicating bpy-RGD had highest affinity for the integrin. As described, bpy-RGD is both more hydrophilic and smaller than dpp-RGD, it is likely therefore to be a better steric fit to the binding pocket. The decrease in K_d observed for dpp-RGD when bound to DTT or Mn^{2+} activated $\alpha_{IIb}\beta_3$ is consistent with this picture, wherein the greater exposure of the RGD pocket in the activated-like conformation of the protein permits deeper penetration by dpp-RGD where conversely activation does not affect K_d for bpy-RGD. Furthermore, the binding curves for dpp-RGD with the resting integrin indicate a more complex interaction than bpy-RGD or dpp-RGD with the activated integrin. This may be suggestive of cooperative binding such as hydrophobic binding which accompanies RGD recognition given the hydrophobicity of this complex. The interactions of RGD probes with integrin have been shown to involve a number of interactions including H-bonding hydrophobic–hydrophobic interactions and electrostatic interactions.[66,75,82,83] However, the long rotational correlation times for dpp-RGD in particular when bound to the resting integrin may indicate that oligomerization of the protein may play a role in this behavior. As described, Hantgan and colleagues have demonstrated that a range of small RGD peptides induce integrin self-association in solution.[58]

Overall, this study shows that the structural status of the integrin can be reported by these long-lived metal complex probes via luminescence lifetime and anisotropy, although the extent of change depends on whether the complex was bound to the integrin before or after activation or denaturation, which suggests the probe plays an active role in controlling the structure of the integrin.

■ CONCLUSIONS

The ability of two novel luminescent Ru(II) polypyridyl peptide conjugates, hydrophilic bpy-RGD and hydrophobic dpp-RGD, to recognize the platelet integrin $\alpha_{IIb}\beta_3$ in solution and in live cells is investigated. Both probes bind selectively to resting $\alpha_{IIb}\beta_3$ with micromolar affinity, reflected in an approximately 8-fold increase in luminescent quantum yield and doubling of luminescent lifetime compared to nonspecific binding to a BSA control. The pharmaceutical integrin inhibitor, Eptifibatide, which recognizes the RGD binding site with high affinity, effectively blocks both bpy-RGD and dpp-RGD from $\alpha_{IIb}\beta_3$ binding, further confirming these complexes' specificity toward the integrin. The long luminescent lifetimes of these complexes make them useful probes of integrin conformation and self-association, as they enable recording of luminescence rotational correlation times over microsecond time scales. On binding to resting $\alpha_{IIb}\beta_3$ in solution, the rotational correlation time of the probes exceeds 1.5 μs, which suggests RGD probe binding induces oligomerization. Probes which can distinguish between different activation states of integrin are potentially very useful, particularly in platelet

dx.doi.org/10.1021/bc5000737 | Bioconjugate Chem. 2014, 25, 928−944

biology, and clear distinctions in terms of association constant, quantum yield, lifetime, and luminescence anisotropy of bpy-RGD and dpp-RGD probe are observed when bound to integrin treated with Mn^{2+}, DTT, or integrin which has been thermally denatured. Interestingly the conformational modifications to the integrin were strongly influenced by whether the bpy-RGD or dpp-RGD already occupied the integrin binding site prior to its chemical activation. Again, this indicates that the RGD probes play a role in modulating the structure or oligomerization of the integrin.

Finally, both bpy-RGD and dpp-RGD bind specifically to $\alpha_{IIb}\beta_3$ in live CHO cells expressing the integrin as confirmed by their colocalization with the SZ22 α_{IIb} integrin specific antibody. The parent dyes without the peptide do not bind to these or the wild type CHOs, and neither bpy-RGD nor dpp-RGD exhibit significant staining of wt-CHO cells not expressing $\alpha_{IIb}\beta_3$.

Integrins are key therapeutic targets in many inflammatory and vascular disorders. Platelet activation during thrombosis is accompanied by integrin conformational change and clustering at the platelet membrane. There is a need for a simple means of evaluating the structural status of integrins in solution, platelets and live cells both for diagnostic assays as well as in fundamental studies into integrin behavior. The ruthenium polypyridyl peptides presented here seem suited to such investigations. We have shown that their photophysical characteristics, polarization, lifetime, and quantum yield, are sensitive to integrin conformational status and that they readily recognize integrin in their native environment. Future work will focus on evaluating these and related probes in platelet integrin in more biorelevant conditions, both in model membranes and in cells, and in building greater specificity into the targeting peptides.

EXPERIMENTAL PROCEDURES

Materials. 1,10-Phenanthroline 5,6-dione (phendione), 2,2′-bipyridine, 4-carboxy benzaldehyde, ammonium acetate, glacial acetic acid, lithium chloride, ruthenium(III)-chloride trihydrate ($RuCl_3{\cdot}3H_20$), 4,7-diphenyl-1,10 phenanthroline (dpp), anhydrous *N,N*-dimethylformamide (DMF), lithium perchlorate, *N*-hydroxysuccinimide (NHS), *N,N′*-dicyclohexylcarbodimide (DCC), amicon ultra centrifugal filter units, MWCO 30 Kda, DMEM nutrient mixture F-12 HAM media, 100 mL accutase, 1 mg/mL G418 a, and 500 mL 37% formaldehyde solution were purchased from Sigma-Aldrich. CD41 and PAC-1 antibodies were purchased from BD Biosciences. G-Ahx-GRGDS peptide was made to order by Celtek Biosciences. G-Ahx-GRGDS identity and purity was manufacturer guaranteed, confirmed by MALDI-TOF-MS and HPLC (Supporting Information). Eptifibatide (*N*6-(amino-iminomethyl)-*N*2-(3-mercapto-1-oxopropyl-L-lysylglycyl-L-α-aspartyl-L-tryptophanyl-L-prolyl-cysteinamide, cyclic (1−6)-disulfide) (also known as Integrilin) was purchased from Peptides International. Eptifibatide identity and purity was manufacturer guaranteed, and confirmed by MALDI-TOF-MS and HPLC (Supporting Information). Purified human platelet glycoprotein integrin $\alpha_{IIb}\beta_3$ was purchased from Enzyme Research Laboratories. Fetal calf serum was purchased from Biosera. CD41 (clone SZ22) monoclonal antibody was obtained from Beckman Coulter. Secondary goat anti-mouse IgG Alexa Fluor 488 and 250 μg/mL Zeocin were obtained from Invitrogen. ESI-MS and MALDI-TOF were measured in the CSCB facility in University College Dublin (UCD), Ireland. ^1H NMR and ^{13}C spectra were recorded on a Brüker AC 400 MHz spectrometer using deuterated DMSO-d_6 as solvent for homonuclear lock. Peak positions are relative to TMS (0 ppm chemical shift). All NMR spectra were analyzed using Topspin NMR software.

Synthesis. *Preparation of 2-(4-Carboxyphenyl)imidazo-[4,5-f][1,10]phenanthroline [PIC] (**1**).* The compound was synthesized according to a method modified from the literature.[84] 0.42 g (2 mmol) of phendione, 0.36 g (2.4 mmol) of 4-carboxybenzaldehyde, and 3.08 g (40 mmol) of ammonium acetate were refluxed in 50 mL glacial acetic acid at 160 °C for 3 h. The solution was allowed to cool to room temperature. The addition of water aided precipitation. The solid was filtered and washed with cold water, methanol, and diethyl ether. The material was lyophilized to yield the ligand as a yellow solid (0.54 g, 79%). Molecular weight: 340 g/mol. ^1H NMR (DMSO-d_6): δ (ppm) 13.96 (s, 1H), 13.04 (s-broad, 1H), 9.06 (d, 2H), 8.95 (d, 2H, J = 8 Hz), 8.42 (d, 2H, J = 8.4 Hz), 8.19 (d, 2H, J = 8.4 Hz), 7.88 (m, 2H).

*Preparation of $[Ru(bpy)_2Cl_2]$ (**2**).* The compound was prepared according to a method modified from the literature.[85] 0.50 g (1.91 mmol) of $RuCl_3{\cdot}3H_2O$ was dissolved in 7 mL anhydrous DMF in a three neck round bottomed flask. 0.55 g (13.00 mmol) of lithium chloride was added to the solution, followed by 0.59 g (3.82 mmol) of 2,2-bipyridine in three equal portions. The reaction was refluxed under a nitrogen environment at 160 °C for 8 h. Acetone was then added to promote precipitation and left in the fridge overnight. The precipitate was collected by vacuum filtration and washed well with acetone and diethyl ether to leave a dark purple colored solid. The product was purified on a silica chromatographic column using 10% methanol−dichloromethane as mobile phase. The material was lyophilized to yield the product as a dark purple solid (0.30 g, 62%). ^1H NMR (DMSO-d_6): d (ppm) 9.94 (d, 2H, J = 4.8 Hz), 8.60 (d, 2H, J = 8 Hz), 8.45 (d, 2H, J = 8.4 Hz), 8.03 (t, 2H, J = 6.4 Hz), 7.74 (t, 2H, J = 6.4 Hz), 7.64 (t, 2H, J = 6.4 Hz), 7.47 (d, 2H, J = 5.2 Hz), 7.07 (t, 2H, J = 6.4 Hz).

*Preparation of $[Ru(bpy)_2(PIC{-}COOH)]^{2+}.(ClO_4)_2$ (**2a**).* The compound was prepared according to a method modified from the literature.[85] 0.03 g (0.123 mmol) of **1**, 0.05 g (0.103 mmol) of **2**, and 15 mL ethanol were placed in a 50 mL round bottomed flask and refluxed at 160 °C for 18 h. The solvent was evaporated under reduced pressure and the crude product was suspended in a saturated solution of lithium perchlorate and filtered. The precipitate was washed with deionized water, diethyl ether, and dichloromethane to yield an orange/red solid. The product was then dissolved in acetonitrile. The precipitate was then removed and the solvent was evaporated to dryness to give an orange/red colored product (69 mg, 87%). ^1H NMR (DMSO-d_6): d (ppm) 14.43 (s, 1H), 9.11 (d, 2H, J = 8.4 Hz), 8.85 (d, 2H, J = 8 Hz), 8.81 (d, 2H, J = 8 Hz), 8.43 (d, 2H, J = 8.4 Hz), 8.20 (m, 4H), 8.11 (t, 2H, J = 6.4 Hz), 8.08 (m, 2H), 7.92 (m, 2H), 7.83 (d, 2H, J = 5.2 Hz), 7.59 (m, 4H), 7.33 (t, 2H, J = 6 Hz). ^{13}C NMR (DMSO-d_6): 24.71, 25.36, 33.16, 50.08, 58.16, 76.83, 77.03, 77.24, 127.19, 127.66, 129.65, 150.87, 154.27. HRMS (ESI): 753.2 m/z observed, 753.77 m/z calculated.

*Preparation of $[Ru(bpy)_2(PIC\text{-}NHS)]^{2+}$ (**2b**).* The compound was prepared according to a method modified from the literature.[85] 0.05 g (0.06 mmol) of **2a**, 0.05 g (0.43 mmol) of NHS, and 0.08 g (0.38 mmol) of DCC were dissolved in 10 mL anhydrous acetonitrile and allowed stir at room temperature for

dx.doi.org/10.1021/bc5000737 | Bioconjugate Chem. 2014, 25, 928−944

4−6 h. The product was purified by column chromatography on alumina using methanol−dichloromethane (1:9 v/v) as eluent. The material was lyophilized yielding an orange/red solid (0.038 g, 75%). ^{1}H NMR (DMSO-d_6): δ (ppm) 14.73 (s, 1H), 9.13 (t, 2H, J = 6 Hz), 8.87 (d, 2H, J = 5.6 Hz), 8.84 (d, 2H, J = 4.8 Hz), 8.57 (d, 2H, J = 5.2 Hz), 8.40 (d, 2H, J = 5.6 Hz), 8.22 (t, 2H, J = 5.2 Hz), 8.11 (m, 4H), 7.98 (m, 2H), 7.84 (d, 2H, J = 3.6 Hz), 7.61 (m, 4H), 7.35 (t, 2H, J = 4.8 Hz). ^{13}C NMR (DMSO-d_6): 30.04, 30.73, 35.76, 42.03, 65.39, 65.47, 127.93, 138.06, 162.28, 171.59, 172.11. HRMS (ESI): 850.14 m/z (M^+) observed, 850.84 m/z (M^+) calculated.

*Preparation of [Ru(dpp)$_2$Cl]$^{2+}$ (**3**).* The compound was synthesized according to a method modified from the literature.[86] 0.10 g (0.38 mmol) of $RuCl_3 \cdot 3H_2O$, 0.25 g (0.76 mmol) of dpp, and 0.11 g (2.66 mmol) of lithium chloride were dissolved in 20 mL anhydrous DMF and refluxed at 200 °C under N_2 until the reaction mixture turned dark purple (4−6 h). The product was purified on a silica chromatographic column using 10% methanol−dichloromethane as mobile phase. The material was lyophilized to yield a dark purple solid (0.20 g, 63%). Molecular weight: 836 g/mol. ^{1}H NMR (DMSO-d_6): δ (ppm) 10.42 (d, 2H, J = 5.2 Hz), 8.26 (dd, 2H, J = 5.6, 9.2 Hz), 8.07 (dd, 6H, J = 9.6, 5.6 Hz), 7.85 (d, 4H, J = 7.2 Hz), 7.74 (m, 6H, J = 6 Hz), 7.56 (m, 10H, J = 6 Hz), 7.40 (d, 2H).

*Preparation of [Ru(dpp)$_2$(PIC−COOH)]$^{2+}\cdot(ClO_4)_2$ (**3a**).* The compound was synthesized according to a method modified from the literature.[87] 0.095 g (0.30 mmol) of **1** and 0.20 g (0.23 mmol) of **3** were refluxed in 30 mL ethanol:water (1:2) at 100 °C for 48 h. The solvent was evaporated under reduced pressure and the crude product was suspended in a saturated solution of lithium perchlorate and filtered. The product was purified on a silica chromatographic column using 10% methanol−dichloromethane as mobile phase. The material was lyophilized to yield an orange solid (0.15 g, 59%). ^{1}H NMR (DMSO-d_6): δ (ppm) 14.55 (s, 1H), 9.11 (d, 2H, J = 8.4 Hz), 8.45 (d, 2H, J = 8.4 Hz), 8.33 (d, 2H, J = 5.6 Hz), 8.24 (m, 3H), 8.14 (dd, 2H J = 8 Hz), 7.85 (t, 2H, J = 5.6 Hz), 7.80 (d, 2H, J = 5.2 Hz), 7.75 (d, 2H, J = 5.6 Hz), 7.61 (m, 24H). ^{13}C NMR (DMSO-d_6): 25.72, 67.61, 126.61, 127.10, 128.69, 128.75, 129.76, 130.27, 120.48, 130.57, 136.02, 136.06, 145.85, 148.43, 148.54, 148.66. HRMS (ESI): 1105.2530 m/z observed, 1105.2631 m/z calculated.

*Preparation of [Ru(dpp)$_2$(PIC-NHS)]$^{2+}$ (**3b**).* 0.20 g (0.23 mmol) of **3a**, 0.05 g (0.43 mmol) of NHS, and 0.08 g (0.38 mmol) of DCC were dissolved in 30 mL anhydrous acetonitrile and allowed stir at room temperature for 4−6 h. The product was purified on a silica chromatographic column using 10% methanol−dichloromethane as mobile phase. The material was lyophilized to yield the complex as a dark orange/red solid (0.21 g, 75%). ^{1}H NMR (DMSO-d_6): δ (ppm) 14.73 (s, 1H), 9.14 (d, 2H, J = 8 Hz), 8.57 (d, 2H, J = 8.4 Hz), 8.38 (2, 2H, J = 5.6 Hz), 8.32 (d, 2H, J = 5.2 Hz), 8.25 (m, 3H), 7.94 (t, 2H, J = 6.4 Hz), 7.80 (d, 2H, J = 5.6 Hz), 7.75 (d, 2H, J = 5.2 Hz), 7.61 (m, 24H). ^{13}C NMR (DMSO-d_6): 24.43, 25.19, 25.72, 25.51, 33.31, 47.46, 128.05, 128.12, 129.15, 129.67, 129.86, 129.94, 135.42, 147.93, 148.00, 156.57, 170.298, 172.79. HRMS (ESI): 1202.5062 m/z observed, 1203.2795 m/z calculated.

Peptide Coupling. *Coupling of G-Ahx-GRGDS to [Ru(bpy)$_2$(PIC-NHS)]$^{2+}$:[Ru(bpy)$_2$ (PIC-RGD)]$^{2+}$; bpy-RGD (**4a**).* 0.02 g (0.016 mmol) of **2b** was dissolved in the minimum amount of degassed anhydrous DMF (~500 μL). 0.04 g (0.006 mmol) of commercial amine terminated G-Ahx-GRGDS peptide was dissolved in 4.5 mL degassed PBS, pH 7.4, and added to the dissolved ruthenium complex. The mixture was stirred under nitrogen for 4 h at room temperature. The product was purified on a silica chromatographic column using 10% methanol−dichloromethane as mobile phase. The product was purified on a silica chromatographic column using 10% methanol−dichloromethane as mobile phase. The material was lyophilized to yield an orange solid (0.012 g, 57%). ^{1}H NMR (400 MHz, DMSO-d_6): d (ppm) 14.27 (s, 1H), 9.12 (d, 2H, J = 8.4 Hz), 8.86 (d, 2H, J = 8 Hz), 8.58 (d, 2H, J = 8 Hz), 8.34 (d, 2H, J = 8.4 Hz), 8.21 (m, 4H), 8.10 (t, 2H, J = 6.4 Hz), 8.08 (m, 2H), 7.96 (m, 2H), 7.84 (d, 2H, J = 5.2 Hz), 7.60 (m, 4H), 7.34 (t, 2H, J = 6 Hz). ^{13}C NMR (DMSO-d_6): 29.99, 60.41, 65.41, 68.11, 70.52, 71.78, 73.16, 75.15, 77.63, 79.86, 86.82, 103.77, 135.95, 143.09, 171.60, 172.18. HR-MALDI-TOF: 1397.23 m/z observed, 1397.09 m/z calculated.

*Coupling of G-Ahx-GRGDS to [Ru(dpp)$_2$(PIC-NHS)]$^{2+}$:[Ru(dpp)$_2$(PIC-RGD)]$^{2+}$, dpp-RGD (**4b**).* 0.02 g (0.016 mmol) of **3b** was dissolved in the minimum amount of degassed anhydrous DMF (500 μL). 0.04 g (0.006 mmol) of G-Ahx-GRGDS was dissolved in 4.5 mL degassed PBS pH 7.4 and quickly added to the dissolved ruthenium. The mixture was stirred for 4−6 h at room temperature. The product was purified on a silica chromatographic column using 10% methanol−dichloromethane as mobile phase. The material was lyophilized to yield an orange solid (0.015 g, 57%). ^{1}H NMR (DMSO-d_6): δ (ppm) 14.55 (s, 1H), 9.12 (d, 2H, J = 8.4 Hz), 8.46 (d, 2H, J = 8.4 Hz), 8.34 (d, 2H, J = 5.6 Hz), 8.25 (m, 3H), 8.15 (dd, 2H J = 8 Hz), 7.87 (t, 2H, J = 5.6 Hz), 7.81 (d, 2H, J = 5.2 Hz), 7.76 (d, 2H, J = 5.6 Hz), 7.63 (m, 24H). ^{13}C NMR (DMSO-d_6): 24.43, 25.27, 33.31, 47.45, 126.03, 126.48, 128.10, 129.13, 129.65, 129.87, 129.95, 135.39, 135.43, 148.02. HR-MALDI-TOF: 1748.6201 m/z observed, 1748.5716 m/z calculated.

Photophysical Measurements. Emission spectra were recorded on a Cary Eclipse Varian luminescence spectrophotometer with a 4 mm × 10 mm quartz cuvette and a slit width of 10 nm for excitation and emission. Quantum yields were calculated according to a standard protocol.[88] This method involves measuring the integrated emission intensity of sample solutions with absorbance at five points between 0.02 and 0.10. This is repeated for a standard of known quantum yield (in this case $[Ru(bpy)_3]^{2+}$). A calibration curve is then prepared and the sample quantum yield estimated using the following relationship:

$$\phi_{Sample} = \phi_{Standard} \times (SLOPE_{Sample}/SLOPE_{Standard}) \quad (1)$$

Time-resolved emission lifetime and anisotropy measurements were carried out on a PicoQuant Fluotime 100 time-correlated single photon counting (TCSPC) system ($\lambda_{exc.}$ 485 nm) using a Thurlby Thandar Instruments (TTi) TGP110 10 MHz pulse generator. For anisotropy measurements sheet polarizers were used to select V polarized excitation from the diode source and the G-factor was estimated by tail matching the VV and VH emission decays. An average of three measurements was taken for each sample, and the data were fit using Fluofit software with a single decay function tail fitting.

Time resolved luminescence anisotropy measurements were analyzed to yield anisotropy (rotational correlation time, t_{rot}) values using the monoexponential model shown in eq 2 using Fluofit software:

$$r(t) = r_0 \exp(-\tau/\tau_{rot}) \quad (2)$$

dx.doi.org/10.1021/bc5000737 | Bioconjugate Chem. 2014, 25, 928−944

where $r(t)$ is the time dependent anisotropy, r_0 is the initial anisotropy, τ is the luminescent lifetime of the sample. Because of the long time-scale of the anisotropy decay and consequently the relatively low resolution of the data over short time-scales, a tail fit rather than reconvolution was used to fit the anisotropy data according to this model. The r_0 depends on the data point from which the fit commences and therefore is not reliably determined from this method so these values are not quoted here.

Protein and Ru-RGD final concentrations for emission and time-resolved emission anisotropy studies were approximately 1.1−0.8 μM ($\alpha_{IIb}\beta_3$: Ru-RGD ratios ranged from 1 to 1.3:1). The same sample and cuvette were used for recording luminescence spectra and luminescent decay data.

Integrin $\alpha_{IIb}\beta_3$ Preparation. Purified human platelet glycoprotein integrin $\alpha_{IIb}\beta_3$ was purchased from Enzyme Research Laboratories. Glycerol was removed from the sample by dilution 2:1 into TrisHCl buffer (150 mM NaCl, 1 mM $CaCl_2$, 20 mM TrisHCl, pH 7.4). Concentration and buffer exchange was achieved using an amicon ultra centrifugal filter unit (MWCO 30 kDa). The diluted $\alpha_{IIb}\beta_3$ protein (3 mL sample volume) was centrifuged at 4000 rpm until approximately 500 μL remained in the filter. Two volumes of buffer were added to the sample and centrifuged again at 4000 rpm. This step was repeated at least three times. The resulting protein sample (approximately 500 μL) concentration was determined using absorption spectrometry ($A_{protein}$ = 280 nm). The sample was stored at 4 °C until required.

Peptide Binding and Activation Studies of Integrin $\alpha_{IIb}\beta_3$. *Mn^{2+} and DTT.* The binding of bpy-RGD or dpp-RGD to $\alpha_{IIb}\beta_3$ was investigated by titrating $\alpha_{IIb}\beta_3$ (2.3 μM stock concentration) TrisHCl buffer (150 mM NaCl, 1 mM $CaCl_2$, 20 mM TrisHCl, pH 7.4) into 500 μL of bpy-RGD or dpp-RGD (2.3 μM stock concentration). The emission from the complex was excited at 450 nm and the corresponding binding curves generated from changes to the peak emission intensity at approximately 610 nm. The effect of activation on the binding of the RGD containing dye was also investigated using the known activating reagents: DTT and $MnCl_2$ (Mn^{2+}). The concentration of reagent used was 10:1 (DTT or Mn^{2+}: $\alpha_{IIb}\beta_3$). The DTT and Mn^{2+} were added either before and after $\alpha_{IIb}\beta_3$ was bound to the ruthenium-RGD probes. Control experiments were also carried out in the same manner to assess any contribution from nonspecific binding using bpy-RGD or dpp-RGD alone, BSA and Eptifibatide (2.3 μM stock concentration in all cases).

Determination of Dissociation Constant K_d. The binding of the bpy-RGD or dpp-RGD to integrin $\alpha_{IIb}\beta_3$ was determined using SigmaPlot 12.0 software (license no 775212810). Binding was analyzed using the equation for the binding of a ligand to a single binding site, fitting the experimental data with eq 3 in order to obtain the dissociation constant value (K_d). This equation is derived from the definition of the dissociation constant, $K_d = R.L/RL$, and the mass balance equation, $R_0 = R + RL$, where R is the concentration of the integrin receptor and L represents the concentration of the ligand, bpy-RGD or dpp-RGD: RL represents the receptor ligand complex.[89]

$$RL = \frac{R_O L}{K_D + L} \quad (3)$$

Cell Culture. Chinese hamster ovary cells (CHO-K1, ATCC no. CCL-61), wild type, CHO-WT, or CHO, transfected with $\alpha_{IIb}\beta_3$ (CHO- $\alpha_{IIb}\beta_3$) were grown in DMEM nutrient mixture F-12 HAM media supplemented with 10% fetal calf serum, 1 mg/mL G418 and 250 μg/mL Zeocin at 37 °C with 5% CO_2. A FACS Calibur instrument was used as a quick and reliable method to quantify the percentage expression of integrin $\alpha_{IIb}\beta_3$ on two transfected CHO cell types: MOCK (no integrin) and WT (resting integrin). Two FITC labeled antibodies were used: CD41 (binds to resting and activated $\alpha_{IIb}\beta_3$) and PAC-1 (binds to activated $\alpha_{IIb}\beta_3$). Cells were detached from culture using Accutase and resuspended in 100 μL PBS, resulting in a total cell count of $\sim 1 \times 10^5$. 50 μL of cells was added to FACS tubes, followed by 50 μL of the desired FITC labeled antibody and then incubated at 37 °C for 10 min. Ice-cold PBS was then added to stop the reaction. FITC was excited at 490 nm and emission monitored at 520−540 nm.

Cell Localization Studies. To investigate the localization of bpy-RGD or dpp-RGD within cell organelles, cells were harvested after accutase treatment and seeded at 1×10^5 cells per well on glass coverslips in 24-well plates. For confocal microscopy measurements, the growth medium was removed from cells grown to 50% confluence, by washing with PBS buffer (pH 7.4, with $MgCl_2$ and $CaCl_2$). Parent dyes (containing no peptide), $[Ru(bpy)_2PIC]^{2+}$ or $[Ru(dpp)_2PIC]^{2+}$ (70 μM) and dye−peptide conjugates bpy-RGD or dpp-RGD (70 μM) were added to each well containing cells and incubated for 4 h at 37 °C. Cells were washed with PBS, fixed with 3.8% PFA solution for 10 min, and blocked with 1.5% BSA for 2 h at room temperature. Cells were stained with a 1:250 dilution of a 0.2 mg/mL stock of CD41(SZ22) antibody in PBS (pH 7.4) overnight at 4 °C followed by a 1:500 dilution of secondary goat anti-mouse IgG Alexa Fluor 488 antibody for 2 h at room temperature. Luminescence images were recorded on a Zeiss LSM510 Meta Confocal microscope using a 64× oil immersion objective lens (NA 1.4).

■ ASSOCIATED CONTENT

Supporting Information

Reaction schemes and photophysical characteristics of the complexes listed. Certificates of analysis of both commercial peptides: G-Ahx-GRGDS and Eptifibatide mimic. NMR and high resolution mass spectrometry data for all synthesized complexes. UV−vis spectra confirming changes in emission were not a result of change in concentration. Flow cytometry confirming the % integrin expression on transfected CHO cells. Luminescence confocal images confirming minimal dye staining of the parents $[Ru(bpy)_2PIC]^{2+}$ and $[Ru(dpp)_2PIC]^{2+}$ and peptide-conjugates bpy-RGD and dpp-RGD of CHO-WT cells and minimal staining of $[Ru(bpy)_2PIC]^{2+}$ and $[Ru(dpp)_2PIC]^{2+}$ in CHO-$\alpha_{IIb}\beta_3$resting integrin expressing cells. Examples of emission anisotropy decay curves and fractional components of all integrin binding studies. This material is available free of charge via the Internet at http://pubs.acs.org.

■ AUTHOR INFORMATION

Corresponding Author

*E-mail: tia.keyes@dcu.ie.

Notes

The authors declare no competing financial interest.

■ ACKNOWLEDGMENTS

The Health Research Board is gratefully acknowledged as this material is based upon work supported by the Health Research Board funded Scholarship program located in the Royal College of Surgeons in Ireland (Award No. PHD/2007/11). This material is based upon work also supported by the Science Foundation Ireland under Grant No. [10/IN.1/B3025] and the National Biophotonics and Imaging Platform, Ireland, and funded by the Irish Government's Programme for Research in Third Level Institutions, Cycle 4, Ireland's EU Structural Funds Programmes 2007−2013.

■ ABBREVIATIONS

bpy-RGD, $[Ru(bpy)_2PIC\text{-}RGD]^{2+}$; dpp-RGD, $[Ru(dpp)_2PIC\text{-}RGD]^{2+}$; RGD, arginine/glycine/aspartic acid; TCSPC, time-correlated single photon counting; χ_r^2, reduced chi-square value; DTT, dithiothreitol; Mn^{2+}, manganese dichloride; CHO, Chinese hamster ovary cells; FACS, fluorescence activated cell sorting; λ_{exc}, excitation wavelength maxima; λ_{em}, emission wavelength maxima; dpp, 4,7-diphenyl-1,10-phenanthroline; PIC, 2-(4-carboxy Pphenyl)imidazo[4,5-*f*][1,10]-phenanthroline

■ REFERENCES

(1) Bennett, J. S., Berger, B. W., and Billings, P. C. (2009) *J. Thromb. Haemost. 7*, 200−205.
(2) Yan, B., Hu, D. D., Knowles, S. K., and Smith, J. W. (2000) Probing chemical and conformational differences in the resting and active conformers of platelet integrin alpha (IIb) beta (3). *J. Biol. Chem. 275*, 7249−7260.
(3) Zhu, J., Luo, B. H., Xiao, T., Zhang, C., Nishida, N., and Springer, T. A. (2008) Structure of a complete integrin ectodomain in a physiologic resting state and activation and deactivation by applied forces. *Mol. Cells 32*, 849−861.
(4) Humphries, M. J. (2000) Integrin structure. *Biochem. Soc. Trans. 28*, 311−339.
(5) Luo, B.-H., Carmen, C., and Springer, T. (2007) Structural basis of integrin regulation and signalling. *Annu. Rev. Immunol. 25*, 619−647.
(6) Campbell, I. D., and Humphries, M. J. (2011) Integrin structure, activation, and interactions. *CSH Perspectives 4*, 1−14.
(7) Fuss, C., Palmaz, J. C., and Sprague, E. A. (2001) Fibrinogen structure, function, and surface interactions. *Journal of Vascular and Interventional Radiology 12*, 677−682.
(8) Mosesson, M. W. (2005) Fibrinogen and fibrin structure and functions. *J. Thromb. Haemost. 3*, 1894−1904.
(9) Bambace, N. M., and Holmes, C. E. (2011) The platelet contribution to cancer progression. *J. Thromb. Haemost. 9*, 237−249.
(10) Ma, Y. Q., Qin, J., and Plow, E. F. (2007) Platelet integrin alpha(IIb)beta(3): activation mechanisms. *J. Thromb. Haemost. 5*, 1345−1352.
(11) Litvinov, R. I., Nagaswami, C., Vilaire, G., Shuman, H., Bennett, J. S., and Weisal, J. W. (2004) Functional and structural correlations of individual aIIbb3 molecules. *Blood 104*, 3979−3985.
(12) Tiwari, S., Askari, J. A., Humphries, M. J., and Bulleid, N. J. (2011) Divalent cations regulate the folding and activation status of integrins during their intracellular trafficking. *J. Cell Sci. 124*, 1672−1680.
(13) Yan, B., and Smith, J. W. (2001) Mechanism of integrin activation by disulfide bond reduction. *Biochemistry 40*, 8861−8867.
(14) Hantgan, R. R., Rocco, M., Nagaswami, C., and Weisal, J. W. (2001) Binding of a fibrinogen mimetic stabilizes integrin aIIbb3's open conformation. *Protein Sci. 10*, 1614−1626.
(15) Takagi, J., Petre, B. M., Walz, T., and Springer, T. (2002) Global conformational rearrangements in integrin extracellular domains in outside-in and inside-out signaling. *Cell 110*, 599−611.
(16) Hantgan, R. R., Stahle, M. C., Connor, J. H., Horita, D. A., Rocco, M., McLane, M., Yakovlev, S., and Medve, L. (2006) Integrin αIIbβ3: ligand interactions are linked to binding-site remodelling. *Protein Sci. 15*, 1893−1905.
(17) Hantgan, R. R., Stahle, M. C., Connor, J. H., Connor, R. F., and Mousa, S. A. (2006) αIIbβ3 priming and clustering by orally active and intravenous integrin antagonists. *J. Thromb. Haemost. 5*, 542−550.
(18) Gonzalez-Rodriguez, J., Acuna, A. U., Alvarez, M. V., and Jovin, T. M. (1994) Rotational mobility of the fibrinogen receptor glycoprotein IIb/IIIa or integrin.alpha.IIb.beta.3 in the plasma membrane of human platelets. *Biochemistry 33*, 266−274.
(19) Ye, Y., and Chen, X. (2011) Integrin targeting for tumor optical imaging. *Theranostics 1*, 102−126.
(20) Bartholomä, M. D. (2012) Recent developments in the design of bifunctional chelators for metal-based radiopharmaceuticals used in Positron Emission Tomography. *Inorg. Chim. Acta 389*, 36−51.
(21) Gaertner, F. C., Kessler, H., Wester, H. J., Schwaiger, M., and Beer, A. J. (2012) Radiolabelled RGD peptides for imaging and therapy. *Eur. J. Nucl. Med. Mol. Imaging 39*, 126−138.
(22) Kuil, J., Velders, A. H., and van Leeuwen, F. W. B. (2010) Multimodal tumor-targeting peptides functionalized with both a radio- and a fluorescent label. *Bioconjugate Chem. 10*, 1709−1719.
(23) Wang, W., Wu, Q., Pasuelo, M., McMurray, J. S., and Li, C. (2005) Probing for integrin $\alpha v\beta 3$ binding of RGD peptides using fluorescence polarization. *Bioconjugate Chem. 16*, 729−734.
(24) Zhou, Y., Chakrabortv, S., and Liu, S. (2011) Radiolabeled cyclic RGD peptides as radiotracers for imaging tumors and thrombosis by SPECT. *Theranostics 1*, 58−82.
(25) Calvete, J. J., Schafer, W., Mann, K., Henschen, A., and Gonzalez-Rodriguez, J. (1992) Localization of the cross-linking sites of RGD and KQAGDV peptides to the isolated fibrinogen receptor, the human platelet integrin glycoprotein IIb/IIIa. Influence of peptide length. *Eur. J. Biochem. 206*, 759−765.
(26) Kurtz, L., Kao, L., Newman, D., Kurtz, I., and Zhu, Q. (2012) Integrin αIIbβ3 inside-out activation. *J. Biol. Chem. 287*, 23255−23265.
(27) Fernández-Moreira, V., Thorp-Greenwood, F., and Coogan, M. P. (2009) Application of d^6transition metal complexes in fluorescence cell imaging. *Chem. Commun. 46*, 186−202.
(28) Li, L., Szmacinski, H., and Lakowicz, J. R. (1997) Synthesis and luminescence spectral characterizationof long-lifetime lipid metal−ligand probes. *Anal. Biochem. 244*, 80−85.
(29) Piszczek, G. (2006) Luminescent metal-ligand complexes as probes of macromolecular interactions and biopolymer dynamics. *Biochem. Biophys. 453*, 54−62.
(30) Zhang, J., Qi, H., Li, Y., Yang, J., Gao, Q., and Zhang, C. (2008) Electrogenerated chemiluminescence DNA biosensor based on hairpin DNA probe labeled with ruthenium complex. *Anal. Chem. 80*, 2888−2894.
(31) Gill, M. R., and Thomas, J. A. (2012) Ruthenium(II) polypyridyl complexes and DNA—from structural probes to cellular imaging and therapeutics. *Chem. Soc. Rev. 41*, 3179−3192.
(32) Slim, M., and Sleiman, H. F. (2004) Ruthenium(II)−phenanthroline−biotin complexes: synthesis and luminescence enhancement upon binding to avidin. *Bioconjugate Chem. 15*, 949−953.
(33) Zsmacinski, H., Terpetschnig, E., and Lakowicz, J. R. (1996) Synthesis and evaluation of Ru-complexes as anisotropy probes for protein hydrodynamics and immunoassays of high-molecular-weight antigens. *Biophys. Chem. 62*, 109−120.
(34) McConnell, A. J., Lim, M. H., Olmon, E. D., Song, H., Dervan, E. E., and Barton, J. K. (2012) Luminescent properties of ruthenium(II) complexes with sterically expansive ligands bound to DNA defects. *Inorg. Chem. 51*, 12511−12520.
(35) Song, H., Kaiser, J. T., and Barton, J. K. (2012) Crystal structure of delta-[Ru(bpy)2(dppz)]2+ bound to mismatched DNA reveals side-by-side metalloinsertion and intercalation. *Nat. Chem. 4*, 615−620.

(36) Puckett, C. A., and Barton, J. K. (2010) Targeting a ruthenium complex to the nucleus with short peptides. *Bioorg. Med. Chem. 18*, 3564−3569.
(37) Bruijnincx, P. C. A., and Sadler, P. J. (2008) New trends for metal complexes with anticancer activity. *Curr. Opin. Chem. Biol. 12*, 197−206.
(38) Meier, S. M., Novak, M., Kandioller, W., Jakupec, M. A., Arion, V. B., Metzler-Nolte, N., Keppler, B. K., and Hartinger, C. G. (2013) Identification of the structural determinants for anticancer activity of a ruthenium arene peptide conjugate. *Chemistry 19*, 9297−9307.
(39) Corral, E., Hotze, A. C., den Dulk, H., Leczkowska, A., Rodger, A., Hannon, M. J., and Reekijk, J. (2009) Ruthenium polypyridyl complexes and their modes of interaction with DNA: Is there a correlation between these interactions and the antitumor activity of the compounds? *J. Biol. Inorg. Chem. 14*, 439−448.
(40) DeGraff, B. A., and Demas, J. N. (1994) Direct measurement of rotational correlation times of luminescent ruthenium(II) molecular probes by differential polarized phase fluorimetry. *J. Phys. Chem. 98*, 12478−12480.
(41) Ruggi, A., van Leeuwan, F. W. B., and Velders, A. H. (2011) Interaction of dioxygen with the electronic excited state of Ir(III) and Ru(II) complexes: Principles and biomedical applications. *Coord. Chem. Rev. 255*, 2542−2554.
(42) Davies, C. L., Dux, E. L., and Duhme-Klair, A.-K. (2009) Supramolecular interactions between functional metal complexes and proteins†. *Dalton Trans.*, 10141−10154.
(43) Lo, K. W., Lee, T. K. M., Lau, J. S. Y., Poon, W. L., and Cheng, S. H. (2008) Luminescent biological probes derived from ruthenium-(II) estradiol polypyridine complexes. *Inorg. Chem. 47*, 200−208.
(44) Lo, K. W., Choi, A. W., and Law, W. H. (2012) Applications of luminescent inorganic and organometallic transition metal complexes as biomolecular and cellular probes. *Dalton Trans. 41*, 6021−6047.
(45) Muldoon, J., Ashcroft, A. E., and Wilson, A. J. (2010) Selective protein-surface sensing using ruthenium(II) tris(bipyridine) complexes. *Chem.—Eur. J. 16*, 100−103.
(46) Vergara, A., Krauss, I. R., Montesarchio, D., Paduano, L., and Merlino, A. (2013) Investigating the ruthenium metalation of proteins: X-ray structure and raman microspectroscopy of the complex between RNase A and AziRu. *Inorg. Chem. 52*, 10714−10716.
(47) Li, F., Feterl, M., Warner, J. M., Day, A. I., Keene, F. R., and Collins, J. G. (2013) Protein binding by dinuclear polypyridyl ruthenium(II) complexes and the effect of cucurbit[10]uril encapsulation†. *Dalton Trans. 42*, 8868−8877.
(48) Karidi, K., Ypsilantis, K., Papakyriakou, A., and Garoufis, A. (2013) Synthesis and characterization of ruthenium(II)−oligopyridine−peptide conjugates. Interactions of the diasteromeres Δ- and Λ-[Ru(bpy)2(4-COY-4′-Mebpy)]Cl2 (Y = Gly-Lys1-Lys2CONH2, Lys1-Gly-Lys2CONH2, Lys1-Lys2-GlyCONH2) with the oligonucleotide d(5′-CGCGAATTCGCG-3′)2. *J. Inorg. Biochem. 127*, 13−23.
(49) Blackmore, L., Moriarty, R., Dolan, C., Adamson, K., Forster, R. J., Devocelle, M., and Keyes, T. K. (2013) Peptide directed transmembrane transport and nuclear localization of Ru(II) polypyridyl complexes in mammalian cells. *Chem. Commun. 49*, 2658−2660.
(50) Puckett, C. A., and Barton, J. K. (2010) Targeting a ruthenium complex to the nucleus with short peptides. *Bioorg. Med. Chem. 18*, 3564−3569.
(51) Fischer, M. J. (2010) Amine coupling through EDC/NHS: A practical approach. *Methods Mol. Biol. 627*, 55−73.
(52) Hermanson, G. T. (2008) Modification of amines with NHS-aldehydes (SFB and SFPA) in *Bioconjugate Techniques*, pp 1233, Elsevier.
(53) Dolan, C., Moriarty, R., Lestini, E., Devocelle, M., Forster, R. J., and Keyes, T. E. (2013) Cell uptake and cytotoxicity of a novel cyclometalated iridium(III) complex and its octaarginine peptide conjugate. *J. Inorg. Biochem. 119*, 65−74.
(54) Ruggi, A., van Leeuwan, F. W. B., and Velders, A. H. (2011) Interaction of dioxygen with the electronic excited state of Ir(III) and Ru(II) complexes: Principles and biomedical applications. *Coord. Chem. Rev. 255*, 2542−2554.
(55) Kirchhofer, D., Gailit, J., Ruoslahti, E., Grzesiak, J., and Pierschbacher, M. D. (1990) Cation dependant changes in the binding specificty of the platelet receptor GPIIb/IIIa. *J. Biol. Chem. 265*, 18525−18530.
(56) Hsu, C.-C., Chuang, W.-J., Chang, C.-H., Tseng, Y.-L., Peng, H.-C., and Huang, T.-F. (2011) Improvements in endotoxemic syndromes using a disintegrin, rhodostomin, through integrin avb3-dependent pathway. *J. Thromb. Haemost. 9*, 593−602.
(57) Szmacinski, H., Castellano, F. N., Terpetschnig, E., Dattelbaum, J. D., Lakowicz, J. R., and Meyer, G. J. (1998) Long-lifetime Ru II complexes for the measurement of high molecular weight protein hydrodynamics. *Biochim. Biophys. Acta 1383*, 151−159.
(58) Hantgan, R. R., Paumi, C., Rocco, M., and Weisel, J. W. (1999) Effects of ligand-mimetic peptides Arg-Gly-Asp-X (X Phe, Trp, Ser) on αIIbβ3 integrin conformation and oligomerization. *Biochemistry 38*, 14461−14474.
(59) Hantgan, R. R., Lyles, D. S., Mallett, T. C., Rocco, M., Nagaswami, C., and Weisel, J. (2003) Ligand binding promotes the entropy-driven oligomerization of integrin αIIbβ3. *J. Biol. Chem. 278*, 3417−3426.
(60) Hantgan, R. R., Rocco, M., Nagaswami, C., and Weisal, J. W. (2001) Binding of a fibrinogen mimetic stabilizes integrin αIIbβ3′s open conformation. *Protein Sci. 10*, 1614−1626.
(61) Schror, K., and Weber, A.-A. (2003) Comparative pharmacology of GP IIb/IIIa antagonists. *J. Thromb. Thrombolys. 15*, 71−80.
(62) Steiner, B., Cousot, D., Trzeciak, A., Gillessan, D., and Hadváry, P. (1989) Ca^{2+}-dependent binding of a synthetic Arg-Gly-Asp (RGD) peptide to a single site on the purified platelet glycoprotein IIb-IIIa complex. *J. Biol. Chem. 264*, 13102−13108.
(63) Pfaff, M., Tangemann, K., Muller, B., Gurrath, M., Muller, G., Kessler, H., Timple, R., and Engel, J. (1994) Selective recognition of cyclic RGD peptides of NMR defined conformation by αIIbβ3, αVβ3, and α5βl Integrins. *J. Biol. Chem. 269*, 20293−20238.
(64) Litvinov, R. I., Nagaswami, C., Vilaire, G., Shuman, H., Bennett, J. S., and Weisal, J. W. (2004) Functional and structural correlations of individual αIIbβ3 molecules. *Blood 104*, 3979−3985.
(65) Xiong, J. P., Stehle, T., Diefenbach, B., Zhang, R., Dunker, R., Scott, D. L., Joachimiak, A., Goodman, S. L., and Arnaout, M. A. (2001) Crystal structure of the extracellular segment of integrin alpha Vbeta3. *Science 294*, 339−345.
(66) Xiong, J. P., Stehle, T., Zhang, R., Joachimiak, A., Frech, A., Goodman, S. L., and Arnaout, M. A. (2002) Crystal structure of the extracellular segment of integrin alpha Vbeta3 in complex with an Arg-Gly-Asp ligand. *Science 296*, 151−155.
(67) Gailit, J., and Ruoslahti, E. (1988) Regulation of the fibronectin receptor affinity by divalent cations. *J. Biol. Chem. 263*, 12927−12932.
(68) Hautanen, A., Gailit, J., Mann, D. M., and Ruoslahti, E. (1989) Effects of modifications of the RGD sequence and its context on recognition by the fibronectin receptor*. *J. Biol. Chem. 264*, 1437−1442.
(69) Litvinov, R. I., Mekler, A., Shuman, H., Bennett, J. S., Barsegov, V., and Weisel, J. W. (2012) Resolving two-dimensional kinetics of the integrin IIb 3-fibrinogen interactions using binding-unbinding correlation spectroscopy. *J. Biol. Chem. 287*, 35275−35285.
(70) Takagi, J., Petre, B. M., Walz, T., and Springer, T. (2002) Global conformational rearrangements in integrin extracellular domains in outside-in and inside-out signaling. *Cell 110*, 599−611.
(71) Xiong, J. P., Stehle, T., Goodman, S. L., and Arnaout, M. A. (2003) Integrins, cations and ligands: making the connection. *J. Thromb. Haemost. 1*, 1642−1654.
(72) McLane, M. A., Kowalska, M. A., Silver, L., Shattil, S. J., and Niewiarowski, S. (1994) Interaction of disintegrins with the $\alpha_{IIb}\beta_3$ receptor on resting and activated human platelets. *Biochemistry 301*, 429−436.
(73) Bednar, R. A., Lee Gaul, S., Hamill, T. G., Egbertson, M. S., Shafer, J. A., Hartman, G. A., Gould, R. J., and Bednar, B. (1998) Identification of low molecular weight gp iib/iiia antagonists that bind

preferentially to activated platelets. *J. Pharmocol. Exp. Ther. 285*, 1317−1326.
(74) Hu, D. D., White, C. A., Panzer-Knodle, S., Page, J. D., Nicholsen, N., and Smith, J. W. (1999) A new model of dual interacting ligand binding sites on integrin $\alpha_{IIb}\beta_3$*. *J. Biol. Chem. 274*, 4633−4639.
(75) Sanchez-Cortes, J., and Mrksich, M. (2009) The platelet integrin aIIbb3 binds to the RGD and AGD motifs in fibrinogen. *Chem. Biol. 16*, 990−1000.
(76) Kamata, T., Ambo, H., Puzon-McLaughlin, W., Tieu, K. K., Handa, M., Ikeda, Y., and Takada, Y. (2004) Critical cysteine residues for regulation of integrin alphaIIbbeta3 are clustered in the epidermal growth factor domains of the beta3 subunit. *Biochem. J. 378*, 1079−1082.
(77) O'Neill, S., Robinson, A., Deering, A., Ryan, M., Fitzgerald, D. J., and Moran, N. (2000) The platelet integrin αIIbβ3 has an endogenous thiol isomerase activity*. *J. Biol. Chem. 275*, 36984−36990.
(78) Kamata, T., Handa, M., Sato, Y., Ikeda, Y., and Aiso, S. (2005) Membrane-proximal α/β stalk interactions differentially regulate integrin activation*. *J. Biol. Chem. 280*, 24775−24783.
(79) Leane, D., Walsh, G., Moran, N., Forster, R. J., Kenny, D., O'Neill, S., and Keyes, T. E. (2007) Activation induced conformational changes within the platelet integrin aIIbb3 using surface enhanced raman spectroscopy. *Biochemistry 46*, 6429−6436.
(80) Garrigues, H. J., Rubinchikova, Y. R., DiPersio, C. M., and Rose, T. M. (2008) Integrin αVβ3 binds to the RGD motif of glycoprotein B of Kaposi's aarcoma-associated herpesvirus and functions as an RGD-dependent entry receptor. *J. Virol. 82*, 1570−1580.
(81) Schwarz, M., Meade, G., Stoll, P., Ylanne, J., Bassler, N., Chen, Y. C., Hagemeyer, C. E., Ahrens, I., Moran, N., Kenny, D., Fitzgerald, D., Bode, C., and Peter, K. (2006) Conformation-specific blockade of the integrin GPIIb/IIIa a novel antiplatelet strategy that selectively targets activated platelets. *Mol. Med. 99*, 25−33.
(82) Xiao, T., Takagi, J., Coller, B. S., Wang, J. H., and Springer, T. A. (2004) Structural basis for allostery in integrins and binding to fibrinogen-mimetic therapeutics. *Nature 432*, 59−67.
(83) Bella, J., Humphries, M. J. (2005) Cα-H···O=C hydrogen bonds contribute to the specificity of RGD cell-adhesion interactions. *BMC Struct. Biol. 5*.
(84) Pellegrin, Y., Forster, R. J., and Keyes, T. E. (2009) PH dependant photophysics and role of medium on photoinduced electron transfer between ruthenium polypyridyl complex and anthraquinone. *Inorg. Chim. Acta 362*, 1715−1722.
(85) Sullivan, B. P., Salmon, D. J., and Meyer, T. J. (1978) *Mixed phosphine 2,2′-bipyridine complexes of ruthenium*, pp 3334−3341, Vol *17*.
(86) Goldstein, B. M., Barton, J. K., and Berman, H. M. (1986) Crystal and molecular structure of a chiral-specific DNA-binding agent: tris(4,7-diphenyl-1,10-phenanthroline)ruthenium(II). *Inorg. Chem. 25*, 842−847.
(87) Cosgrave, L., Devocelle, M., Forster, R. J., and Keyes, T. E. (2010) Multimodal cell imaging by ruthenium polypyridyl labelled cell penetrating peptides. *Chem. Commun. 46*, 103−105.
(88) Williams, A. T. R., Winfield, S. A., and Miller, J. N. (1983) Relative fluorescence quantum yields using a computer controlled luminescence spectrometer. *Analyst 108*, 1067.
(89) Pederson, S. E., Lurtz, M. M., Papineni, R. V. L. (2010) Ligand binding methods for analysis of ion channel structure and function, in *Essential Ion Methods* (Conn, M. P., Ed.) pp 249, Baker and Taylor.